Review | Open Access

Energy Materials

Song *et al. Energy Mater.* **2026**, *6*, 600145 **DOI:**10.20517/energymater.2026.290

Interface failure behaviors and performance enhancement strategies of graphite anodes for lithium-ion batteries

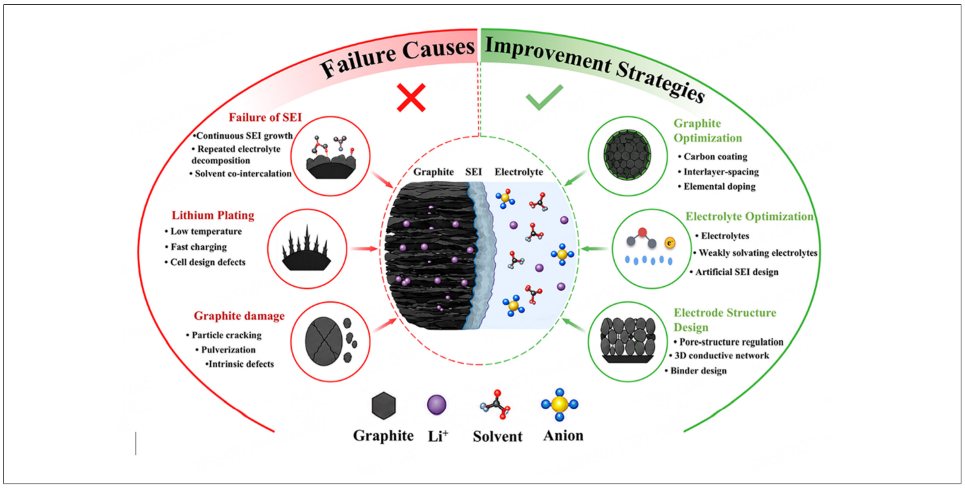
Xuchao Song[1,#], Qifa Chen[2,3,#], Jianghong Wang[2,3], Jinyu Zhao[2,3,4,*], Zhenxin Zhao[1,5,*], Jiajun Chen[1], Xin Liu[5,*], Jiang Ji[2,3,4,*]

Keywords:
Graphite, lithium-ion batteries, failure mechanism

Citation: Song, X.; Chen, Q.; Wang, J.; Zhao, J.; Zhao, Z.; Chen, J.; Liu, X.; Ji, J. Interface failure behaviors and performance enhancement strategies of graphite anodes for lithium-ion batteries. *Energy Mater.* **2026**, *6*, 600145. https://dx.doi.org/10.20517/energymater.2026.290

Received: 27 Aug 2026
First Decision: 21 Sep 2026
Revised: 26 Sep 2026
Accepted: 16 Oct 2026
Published: 27 Oct 2026

Academic Editor: Yuping Wu
Copy Editor: Fangling Lan
Production Editor: Fangling Lan



Abstract

Graphite serves as the mainstream anode material for commercial lithium-ion batteries, benefiting from its superior reversibility, low lithiation potential, and excellent manufacturing compatibility. Nevertheless, its long-term stability is still hindered by the inherently low lithiation potential, uneven interfacial electrochemical activity and structural variation. Notably, the failure behaviors include an unstable solid electrolyte interphase (SEI) film, lithium metal deposition, and mechanical structural damage. This review comprehensively illustrates the structural features and lithium storage mechanisms of graphite anode materials, and systematically analyzes the degradation mechanisms

[1]College of Materials Science and Engineering, Taiyuan University of Technology, Taiyuan 030024, Shanxi, China.
[2]College of Mechanical Engineering, Taiyuan University of Technology, Taiyuan 030024, Shanxi, China.
[3]Engineering Research Center of Advanced Metal Composites Forming Technology and Equipment of Ministry of Education, Taiyuan University of Technology, Taiyuan 030024, Shanxi, China.
[4]National Key Laboratory of Metal Forming Technology and Heavy Equipment, Taiyuan University of Technology, Taiyuan 030024, Shanxi, China.
[5]CNOOC (Shanxi) Precious Metals Co., Ltd., Jinzhong 030600, Shanxi, China.
[#]Authors contributed equally.

[*]**Correspondence to:** Dr. Jinyu Zhao, College of Mechanical Engineering, Taiyuan University of Technology, Taiyuan 030024, Shanxi, China; Engineering Research Center of Advanced Metal Composites Forming Technology and Equipment of Ministry of Education, Taiyuan University of Technology, Taiyuan 030024, Shanxi, China; National Key Laboratory of Metal Forming Technology and Heavy Equipment, Taiyuan University of Technology, Taiyuan 030024, Shanxi, China. E-mail: zhaojinyu@tyut.edu.cn; Dr. Zhenxin Zhao, College of Materials Science and Engineering, Taiyuan University of Technology, Taiyuan 030024, Shanxi, China; CNOOC (Shanxi) Precious Metals Co., Ltd., Jinzhong 030600, Shanxi, China. E-mail: zhaozhenxin@tyut.edu.cn; Dr. Xin Liu, CNOOC (Shanxi) Precious Metals Co., Ltd., Jinzhong 030600, Shanxi, China. E-mail: liuxin47@cnooc.com.cn; Dr. Jiang Ji, College of Mechanical Engineering, Taiyuan University of Technology,

Taiyuan 030024, Shanxi, China; Engineering Research Center of Advanced Metal Composites Forming Technology and Equipment of Ministry of Education, Taiyuan University of Technology, Taiyuan 030024, Shanxi, China; National Key Laboratory of Metal Forming Technology and Heavy Equipment, Taiyuan University of Technology, Taiyuan 030024, Shanxi, China. E-mail: jijiang@sino-heavymach.com

originating from continuous SEI growth and reconstruction, solvent cointercalation, lithium plating, particle fracture, and macroscopic electrode structural evolution. Furthermore, recent research progress on graphite anode modification is summarized. We critically discuss the regulatory effects of the optimization strategies on lithium-ion migration kinetics, interfacial chemical properties, electrode mechanical stability, and spatially inhomogeneous electrochemical response. By correlating degradation mechanisms with multiscale regulation strategies, this review highlights the importance of coordinated optimization across material, interface, particle, and electrode scales for durable graphite anodes. These insights offer perspectives for the development of durable, fast-charging, and safe graphite-based lithium-ion batteries.

INTRODUCTION

Lithium-ion batteries (LIBs) feature high energy density, long cycle life, and low self-discharge, which enable their wide application. They have evolved from conventional portable electronic devices to essential energy storage systems for electric vehicles, large power grids, and aerospace equipment[1,2]. With the development of modern energy storage applications, continuously increasing demands are being placed; traditional LIB technologies are gradually reaching their inherent performance limits[3]. The anode material is a key part of LIBs that enables the reversible storage and release of Li^+. Its structural stability and interfacial behavior directly determine electrochemical performance[4].

Although advanced high-capacity anode materials, such as silicon-based materials and lithium metal, have been widely studied in recent years, graphite is still the most commonly used anode material in commercial LIBs. It possesses favorable characteristics including a low and stable lithiation voltage, good lithium-ion reversibility, and small volume change during cycling. With balanced electrochemical performance, stable structure, and great industrial practicability, graphite remains the mainstream choice for large-scale energy storage, especially in electric vehicles and grid energy storage systems[5].

However, the graphite anode surface is continuously subjected to complex interfacial reactions with the electrolyte, accompanied by irreversible structural and chemical evolution under repeated lithiation/delithiation cycling, temperature variations, and high-rate charging conditions. These interactive negative effects slowly damage the structure and interface stability of graphite anodes. This process triggers continuous, unregulated growth and component changes of the solid electrolyte interphase (SEI), as well as lithium accumulation, lithium dendrite formation, particle breakage and even powdering. It also damages the overall structure of the electrode coating[6-8]. These degradation behaviors are closely linked with each other due to interfacial side reactions, continuous mechanical stress buildup and the repeated exposure of fresh graphite surfaces. This mutual promotion further worsens the electrochemical performance, finally leading to obvious macroscopic problems such as fast capacity loss, rising interface resistance and hidden thermal safety risks. Therefore, it is a critical obstacle to the development of high-performance and highly reliable graphite-based LIBs[9,10].

Considerable effort has been devoted to modifying graphite anodes at the electrolyte, material, and electrode levels[11-13]. Surface carbon layers and heteroatom doping are commonly used to change the chemical environment of graphite and improve its contact with the electrolyte. Electrolyte composition provides another route to influence graphite behavior. Weakly solvating electrolytes and high-concentration formulations change the coordination environment of Li^+, which can affect both the desolvation process and

the composition of the SEI[14,15]. Despite these developments, it is still difficult to anticipate how graphite will degrade during practical battery operation. SEI evolution, mechanical damage, and variations in electrochemical activity do not occur independently, and their relative importance can change with operating conditions. The situation becomes more complicated when moving from laboratory cells to commercial-format batteries, where differences in heat generation and dissipation, mechanical constraint, and current distribution can substantially alter the local reaction environment. As a result, excellent performance in a laboratory cell does not necessarily translate directly to a practical battery[16-18].

This review examines the degradation mechanisms of graphite anodes in LIBs and the approaches developed to mitigate these limitations. The structural characteristics and lithium-storage behavior of graphite are considered to establish the relationship between graphite structure, interfacial chemistry, and electrochemical performance. The discussion then focuses on three closely related degradation processes: SEI instability, lithium plating, and mechanical damage to graphite particles. Their origins and interactions are examined to clarify the progressive degradation of graphite anodes. Recent approaches to improving graphite anode performance are discussed from the perspectives of material engineering, electrolyte chemistry, and electrode architecture, together with the mechanisms underlying their effects. These discussions provide a basis for understanding graphite anode degradation and for developing more durable and safer LIBs.

STRUCTURAL CHARACTERISTICS OF GRAPHITE ANODES

Graphite has a layered structure made up of sp^2-hybridized carbon atoms. Within each layer, the carbon atoms are connected by strong covalent bonds to form a hexagonal network. The interaction between adjacent layers is much weaker and is dominated by van der Waals forces. This difference in bonding strength gives graphite a pronounced structural anisotropy and underlies its characteristic Li-storage behavior[19]. During charging, Li^+ gradually enters the interlayer galleries, and the process is reversed during discharge. The fully lithiated state is commonly represented by LiC_6, giving graphite a theoretical capacity of about 372 mAh g^{-1}[20]. Graphite also operates at a low potential of approximately 0.1 V *vs.* Li^+/Li, which results in its widespread use as an anode in LIBs.

The insertion of Li^+ into graphite is not simply a bulk diffusion process. Before reaching the graphite layers, Li^+ must first shed part of its solvation shell at the electrolyte interface and then cross the SEI. It subsequently reaches the graphite surface and diffuses into the interlayer galleries[21,22]. Thus, the overall kinetics are influenced by interfacial transport, charge transfer, solid-state diffusion, and the architecture of the composite electrode. Unlike conversion-type anodes, which store lithium through multielectron reactions accompanied by phase transformations, graphite relies mainly on reversible Li^+ intercalation between graphene layers and consequently undergoes relatively small structural changes during cycling[23,24]. The relatively small structural change is beneficial for cycling, but the low lithiation potential of graphite leaves only a limited margin before lithium metal can form. This becomes important at high charging rates and low temperatures, where sluggish Li^+ transport can cause the graphite potential to approach the lithium deposition potential[25].

Graphite is not completely free from structural changes during cycling. Li^+ insertion expands the lattice mainly along the c-axis, and Li^+ removal causes it to contract again. The overall volume change is only approximately 10%, considerably smaller than that of alloying anodes such as silicon, but repeating this expansion and contraction still produces mechanical stress inside the particles and across the electrode[26,27]. With continued cycling, the accumulated stress can contribute to crack formation and particle damage. Surface structure adds another layer of complexity. The basal plane of graphite is relatively inactive toward electrolyte reactions, whereas the edge regions are much more reactive and are important sites for electrolyte

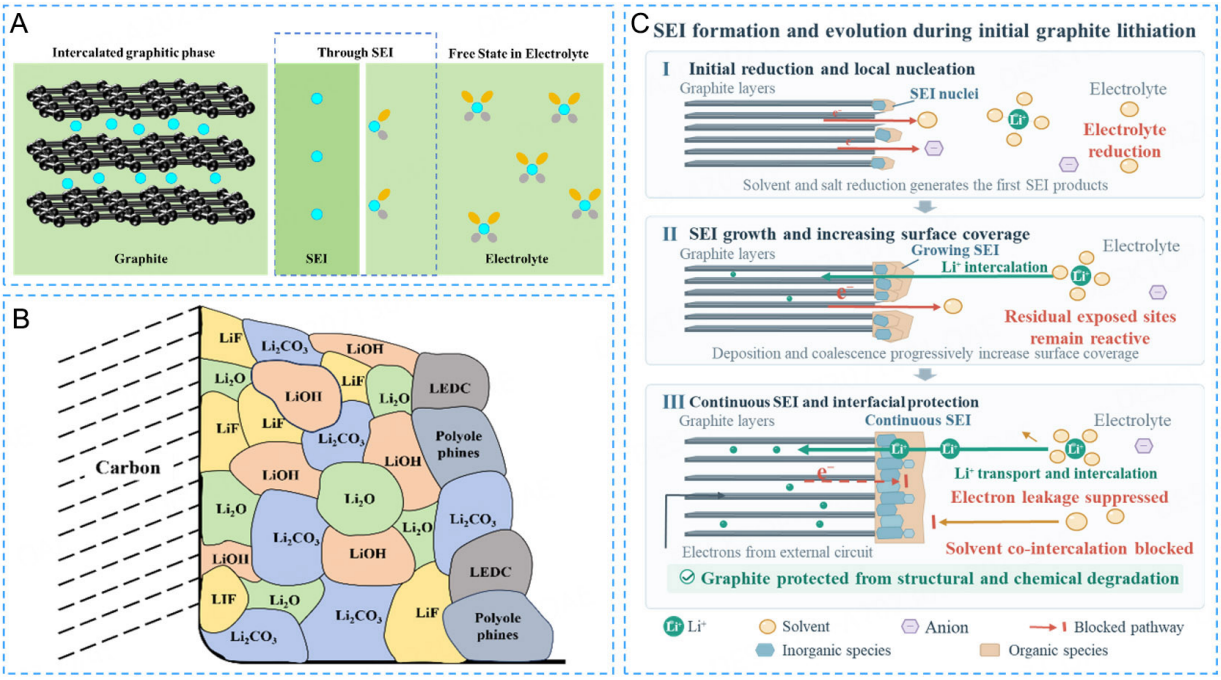


Figure 1. (A) Li^+ transport and intercalation across the graphite anode, SEI, and electrolyte interface. (B) Composition of the SEI. (C) Formation and evolution of the SEI during initial graphite lithiation.

decomposition and SEI formation[28]. A graphite particle therefore does not present a chemically uniform surface to the electrolyte. Differences between basal and edge sites can produce spatial variations in SEI formation and local electrochemical activity. Taken together, the behavior of graphite during cycling depends on more than its bulk crystal structure. Surface reactivity, Li^+ transport, particle mechanics, and the architecture of the electrode all contribute to its long-term degradation.

MAIN FAILURE MECHANISMS OF GRAPHITE

Failure of the SEI film

The SEI is a nanoscale passivation layer formed *in situ* at the electrode/electrolyte interface through the reductive decomposition of electrolyte components at the low potential of the negative electrode[29,30]. During lithium storage, Li^+ initially exists in a solvated state in the electrolyte and undergoes progressive desolvation as it approaches the graphite surface. The resulting desolvated or partially desolvated Li^+ species subsequently traverse the SEI and enter the graphite lattice through interlayer sites, forming lithium-graphite intercalation compounds. The SEI therefore serves as a critical interfacial layer that regulates Li^+ transport across the interface and maintains the stability of the graphite anode [Figure 1A].

The principal components and structural features of the SEI are presented in Figure 1B. An effective SEI should possess a dual functionality: electronic insulation to suppress electron transfer toward the electrolyte, together with sufficient Li^+ conductivity to sustain rapid ionic transport. An effective SEI must electronically isolate the graphite surface to suppress further electrolyte reduction and associated lithium loss, while retaining sufficient Li^+ conductivity for ion transport during cycling and reversible lithium intercalation and deintercalation[31]. The formation and evolution of the SEI during the initial lithiation of graphite are schematically depicted in Figure 1C. From an interfacial kinetic perspective, the SEI also suppresses persistent parasitic reactions between the electrolyte and graphite and prevents the direct cointercalation of solvent molecules, thereby protecting the graphite structure from severe structural and chemical degradation[32].

Despite these protective functions, SEI formation has both beneficial and detrimental effects. During prolonged cycling, its morphology, composition, and thickness continuously evolve through electrochemical reactions, potentially leading to increased interfacial resistance, active lithium loss, and capacity decay[33]. A detailed understanding of SEI formation and failure is therefore essential for constructing stable electrode interfaces and improving the cycling performance of LIBs.

SEI continuous evolution and electrolyte decomposition

Although the initially formed SEI can to some extent passivate the surface of graphite, it is not static and stable during the long-term cycling process. Instead, it continuously evolves under the combined effects of electrolyte reduction, interface layer growth, and mechanical damage[34]. As shown in Figure 2A, transport phenomena like electron tunneling and solvent diffusion further trigger deposition of insoluble species. Thermodynamically, the lithiation potential of graphite, approximately 0.1 V relative to Li^+/Li, is substantially lower than the lower stability limit of conventional carbonate electrolytes, approximately 1.0 V relative to Li^+/Li[35]. The electrolyte therefore remains metastable, making reductive decomposition unavoidable during graphite lithiation. Using ab initio molecular dynamics simulations, Leung *et al.*[36] investigated the decomposition pathways of ethylene carbonate (EC) during the initial formation of the SEI at the graphite/electrolyte interface. Their results identified carbon edge sites as key catalytic centers for EC decomposition and demonstrated that rapid interfacial reduction can occur under experimentally relevant conditions, yielding products including Li_2CO_3, lithium ethylene dicarbonate, C_2H_4, and CO [Figure 2B]. This indicates that SEI formation originates primarily from the highly active interfacial reduction reactions at low potentials, and the differences in reactivity at different sites on the graphite surface further determine the spatial nonuniformity of the initial SEI formation.

Although the SEI is generally regarded as electronically insulating, a small number of electrons can still migrate through the layer by quantum tunneling or along low-resistance pathways. As illustrated in Figure 2C, energy level differences and electron transport barriers exist within the SEI. When the layer is sufficiently thin or contains structural defects, electrons may overcome these barriers and reach the SEI/electrolyte interface, where they induce further reduction of solvent molecules or lithium salt anions. Wang *et al.*[37] adapted a schematic energy-level diagram to illustrate the thermodynamic origin of anode SEI formation, showing that electrolyte reduction occurs when the anode redox potential (μA) lies above the electrolyte lowest occupied molecular orbital, whereas electrolyte oxidation occurs when the cathode redox potential (μC) lies below the electrolyte highest occupied molecular orbital; SEI formation is therefore expected when the electrode potentials fall outside the electrolyte electrochemical stability window (Eg). Lin *et al.*[38] reported an electron tunneling model based on density functional theory (DFT) calculations to evaluate the electronic insulating abilities of SEI components, suggesting that initial irreversible capacity loss is driven by self-limiting electron tunneling. Smeu *et al.*[39] further demonstrated that grain boundaries between SEI components such as LiF can enhance electron tunneling. The resulting insoluble products accumulate on the existing SEI surface, promoting further outward growth and thickening of the interphase.

Li *et al.*[40] employed a single-particle model incorporating both SEI formation and stress-induced cracking, allowing for a systematic identification of the diverse mechanisms driving SEI thickening. Graphite particles experience diffusion-induced stress owing to volume changes. This stress promotes the continued growth of the initial SEI on the particle surface and induces the nucleation and propagation of internal cracks. Edge *et al.*[41] presented a schematic illustration [Figure 2D] to summarize the coupling between particle fracture and SEI growth in anode electrodes, showing that cracks expose fresh electron-conductive surfaces for new SEI formation, and that progressive SEI cracking/regrowth, crack network formation, electrode pulverization, and island formation ultimately lead to loss of active material and loss of lithium inventory. These results highlight that the exposure of fresh surfaces via cracking is a main way of driving rapid SEI thickening and the associated capacity decay.

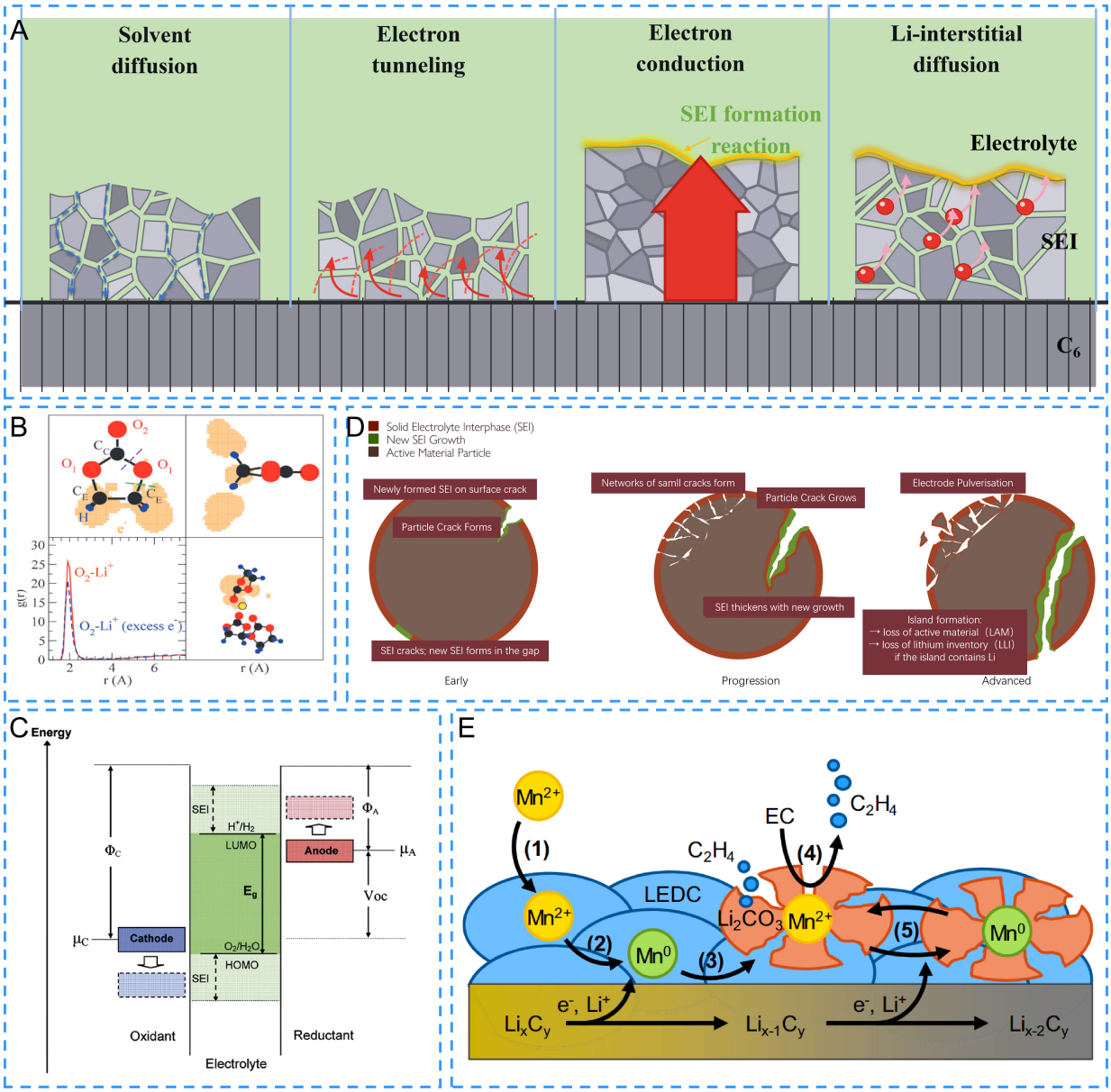


Figure 2. (A) Schematic illustration of four transport mechanisms responsible for SEI growth. (B) Decomposition pathway of EC; (B) is reprinted with permission from Ref.[36], Copyright © 2010, Royal Society of Chemistry. (C) Calculated electron tunneling barrier; (C) Reproduced from Ref.[37], licensed under CC BY 4.0. (D) Coupled evolution of particle cracking, fresh-surface exposure, SEI regeneration, and the loss of active material and lithium inventory; (D) Reproduced from Ref.[41], licensed under CC BY 3.0. (E) C_2H_4 evolution in an Mn^{2+}-containing electrolyte; (E) Reproduced from Ref.[48], licensed under CC BY 4.0.

Once the SEI is disrupted, fresh and highly catalytic graphite surfaces are directly exposed to the electrolyte. Solvent molecules, including EC and ethyl methyl carbonate (EMC), and lithium salt anions, including PF_6^-, can then undergo further reduction at low potentials[42]. The products and reaction pathways associated with recurrent electrolyte reduction are highly complex. Aurbach *et al.*[43] investigated SEI formation on graphite in the presence of vinyl-containing additives using *in situ* Fourier transform infrared spectroscopy and an electrochemical quartz crystal microbalance. They identified cathodically induced vinyl polymerization as the principal reduction pathway of vinyl-containing additives. The reduction potentials of different electrolyte components vary substantially. Additives such as vinylene carbonate are generally reduced

preferentially at relatively high potentials, approximately 1.35 V, whereas the main solvent EC is reduced at approximately 0.8 V. Zhang *et al.*[44] established a controlled experimental system by deliberately adjusting the negative-to-positive electrode capacity ratio. A series of tests were combined to quantify major electrolyte components. These results confirm that the electrolyte decomposition pathway is driven by lithium plating rather than following the conventional pathway associated with anode aging. Furthermore, the results showed that vinylene carbonate was rapidly consumed after controlled lithium plating occurred, whereas PF_6^-, EMC, and EC exhibited time-dependent nonfaradaic consumption. Beyond the mechanisms discussed above, lithium plating and the dissolution of transition metals from the cathode can further accelerate the degradation of the SEI layer. The deposited lithium on the graphite surface will react with electrolyte components, leading to the formation of additional SEI species and continued lithium consumption. In addition, the accumulation and growth of lithium plating can also disrupt the SEI and expose the fresh graphite surfaces. Besides, at elevated temperatures, the SEI becomes less thermally stable, which accelerates the decomposition of its components and promotes further electrolyte reduction[45-47]. Transition metal ions dissolved from the cathode can migrate to the graphite anode and catalyze electrolyte decomposition [Figure 2E]. Electrochemical mass spectrometry showed that ions such as Mn^{2+} promote the decomposition of SEI components, thereby compromising SEI integrity and triggering additional electrolyte reduction[48]

SEI damage and reconstruction induced by solvent cointercalation

In specific electrolyte systems, solvated Li^+ may enter the graphite interlayers before complete desolvation, resulting in solvent cointercalation[49,50]. Solvent molecules may undergo further decomposition within the interlayers and generate gaseous products, producing substantial internal stress that expands the graphite galleries and induces structural degradation, including layer exfoliation and particle pulverization[51]. Meanwhile, interlayer expansion and structural disruption can rupture the preexisting SEI, exposing fresh carbon surfaces to the electrolyte. Further electrolyte reduction then occurs, accompanied by the formation of a new SEI. Repeated SEI reconstruction is therefore induced and is commonly associated with gas evolution, active lithium consumption, and rapid capacity decay. Solvent cointercalation is consequently regarded as an important cause of early graphite anode failure.

In carbonate-based electrolytes, Luchkin *et al.*[52] demonstrated that interfacial enrichment of EC increases the local liquidus temperature and enhances interfacial rigidity, thereby kinetically suppressing the penetration of solvated Li^+ species into graphite during the initial SEI formation process [Figure 3A]. In contrast, this kinetic regulation is absent in propylene carbonate (PC)-based systems, allowing more extensive solvent cointercalation, which leads to severe graphite expansion and SEI fracture along edge planes.

For ether-based electrolytes, strong Li^+-solvent interactions facilitate the cointercalation of Li^+-ether complexes, leading to graphite exfoliation. Chen *et al.*[53] employed a topological molecular engineering strategy to regulate ether solvent structures and systematically elucidated the influence of molecular electronic properties and steric volume on graphite lithiation behavior [Figure 3B]. They found that repeated SEI rupture and reconstruction caused by Li^+/ether cointercalation were the main contributors to capacity loss, indicating a close relationship between solvent cointercalation and interfacial instability in ether-based electrolytes. Beyond conventional ether solvents, Yan *et al.*[54] further demonstrated that reversible solvent cointercalation represents a more general interfacial phenomenon occurring across various electrolyte chemistries. Functional solvents, including trimethyl phosphate, triethyl phosphate, and tetramethylene sulfone, were all found to participate in reversible graphite cointercalation. Their study identified solvent coordinating ability and Li^+ solvation structures as the two key parameters governing the onset potential of solvent cointercalation. By introducing film-forming additives with reduction potentials higher than the cointercalation threshold, such as fluoroethylene carbonate (FEC) and vinyl ethylene carbonate, a robust SEI

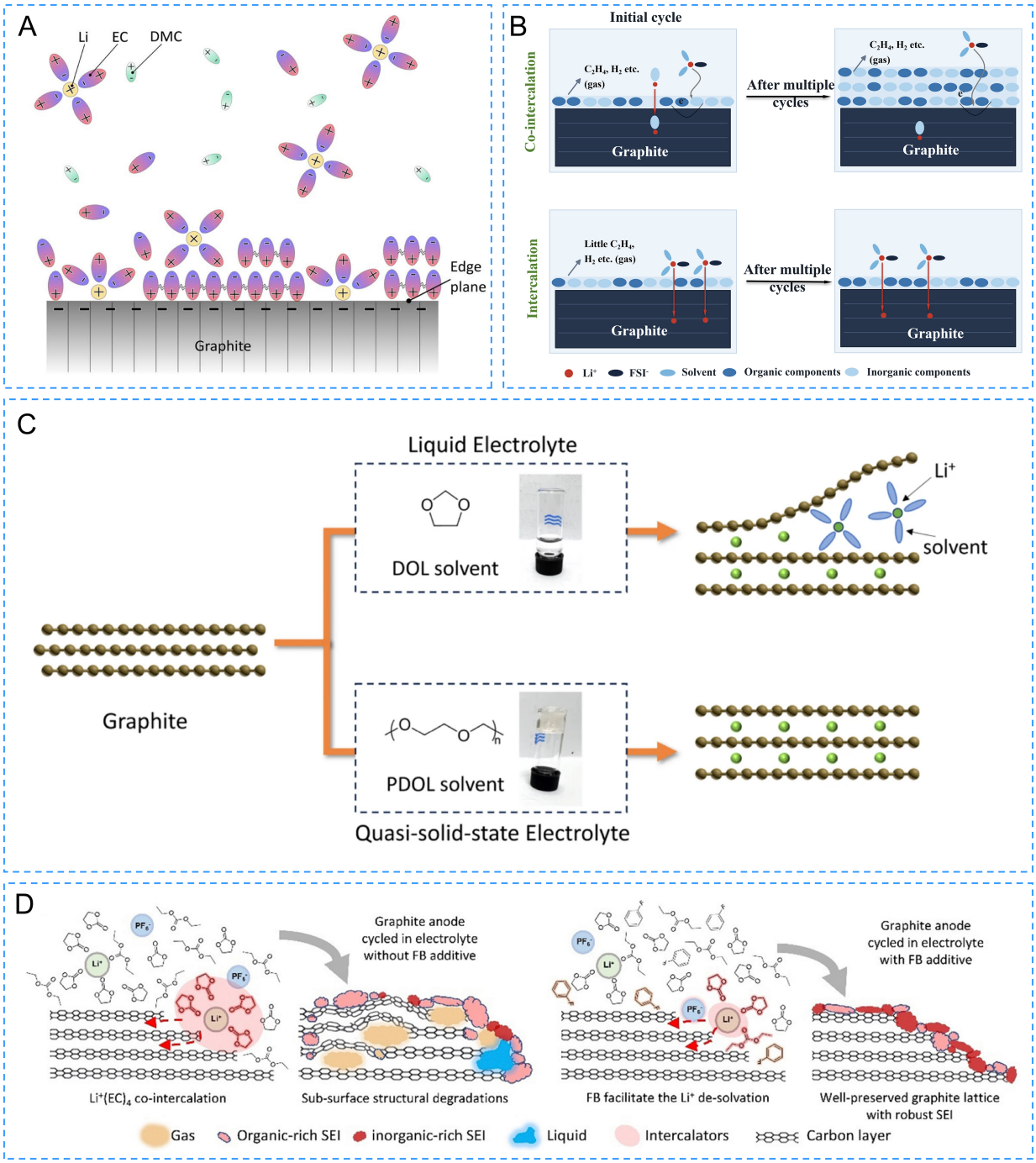


Figure 3. (A) Graphite electrolyte interface enriched with EC molecules; (A) is reprinted with permission from Ref.[52], Copyright © 2024, Royal Society of Chemistry. (B) Schematic comparison of cointercalation-induced SEI disruption and stable Li^+ intercalation during cycling. (C) Comparison of Li^+/1,3-dioxolane (DOL) cointercalation in a liquid electrolyte and suppressed solvent cointercalation in a poly(1,3-dioxolane) (PDOL)-based quasi-solid-state electrolyte; (C) Reproduced from Ref.[55], licensed under CC BY 4.0. (D) Schematic illustration of structural degradation and interfacial chemistry of cycled graphite anodes in electrolytes with and without the FB additive. (D) is reprinted with permission from Ref.[56], Copyright © 2025, Royal Society of Chemistry.

can be preferentially established to prevent solvent penetration and suppress subsequent electrolyte decomposition.

In addition to the preferential formation of a protective SEI, solvent polymerization provides another route to suppress cointercalation. Li *et al.*[55] developed a poly(1,3-dioxolane) (PDOL)-based quasi-solid-state electrolyte for lithium-sulfur batteries with graphite anodes through the *in situ* ring-opening polymerization

of 1,3-dioxolane (DOL), initiated by the metallic 1T-MoS_2 sulfur host. As illustrated in Figure 3C, DOL molecules in the liquid electrolyte can cointercalate with Li^+ into graphite and cause exfoliation. In contrast, the larger molecular size of the resulting PDOL chains hinders their entry into the graphite interlayers, suppressing solvent cointercalation while maintaining reversible Li^+ intercalation and deintercalation. X-ray diffraction (XRD) and Raman analyses further showed that the quasi-solid-state system preserved the graphite structure and mitigated cointercalation-induced exfoliation and disorder. Chen *et al.*[56] employed ultrasound-assisted *in situ* atomic force microscopy to visualize the dynamic evolution of solvent cointercalation, SEI formation, and gas generation in graphite anodes at the nanoscale. The combined atomic force microscopy atomic (AFM) observations and DFT calculations revealed that the cointercalation and interlayer decomposition of $Li^+(EC)_4$ solvation complexes were the primary causes of gaseous cavity formation within the graphite interlayers. These gas bubbles disrupted interfacial stability during battery formation cycles [Figure 3D]. By introducing fluorobenzene, a nonsolvating diluent with a low dielectric constant, the desolvation energy and interfacial molecular configuration were optimized, resulting in the complete suppression of solvent cointercalation and interlayer decomposition.

Lithium plating

Lithium plating refers to the electrochemical reduction of Li^+ to metallic lithium at the graphite/electrolyte interface during charging, followed by the deposition and growth of metallic lithium on the anode surface, typically in dendritic, mossy, or other heterogeneous morphologies. Thermodynamically, the lithiation potential of graphite lies close to the equilibrium potential of the Li^+/Li redox couple (0 V *vs.* Li^+/Li), leaving only a narrow potential margin between lithium intercalation and metallic lithium deposition[57]. Under unfavorable operating conditions, such as low temperature, high-rate charging, or high state of charge, sluggish Li^+ transport and interfacial reaction kinetics increase anode polarization and drive the local graphite potential toward, or below, the Li^+/Li equilibrium potential. Under these conditions, Li^+ reduction to metallic lithium becomes kinetically competitive with its intercalation into the graphite galleries, leading to the accumulation of metallic lithium on the anode surface[57-59].

Lithium plating induced by low temperature

Low temperature is a major factor contributing to lithium plating on graphite anodes. Cooling simultaneously slows Li^+ transport through the electrolyte and across the SEI, as well as solid-state diffusion within graphite particles, while increasing the charge-transfer resistance at the electrode/electrolyte interface. These coupled kinetic limitations substantially increase anode polarization and can drive the local graphite potential toward or below the Li^+/Li equilibrium potential. Once the local potential reaches the lithium plating regime, Li^+ reduction to metallic lithium becomes increasingly favored over intercalation into the graphite lattice[60]. Previous studies have shown that metallic lithium deposition is more likely to occur on graphite anodes during operation or charging at temperatures below 0 °C[61,62].

Cheng *et al.*[63] combined differential voltage analysis, scanning electron microscopy, and Raman spectroscopy to accurately determine the critical depth of discharge and critical potential for the onset of lithium plating at low temperatures [Figure 4A]. Their quantitative analysis showed that the critical potential shifted markedly toward more negative values and the critical depth of discharge decreased sharply as the temperature declined. The study further demonstrated that lithium intercalation is considerably more sensitive to low temperature than lithium deintercalation. This kinetic imbalance can trigger premature lithium deposition, resulting in active lithium loss and capacity decay. Chen *et al.*[64] used three-electrode galvanostatic measurements combined with differential capacity analysis to examine the competition between lithium intercalation and plating from -40 to 30 °C. At temperatures near room temperature, intercalation occurred before the onset of lithium plating. As the temperature decreased below -20 °C, however, the two reactions increasingly overlapped and proceeded simultaneously, indicating a shift in the

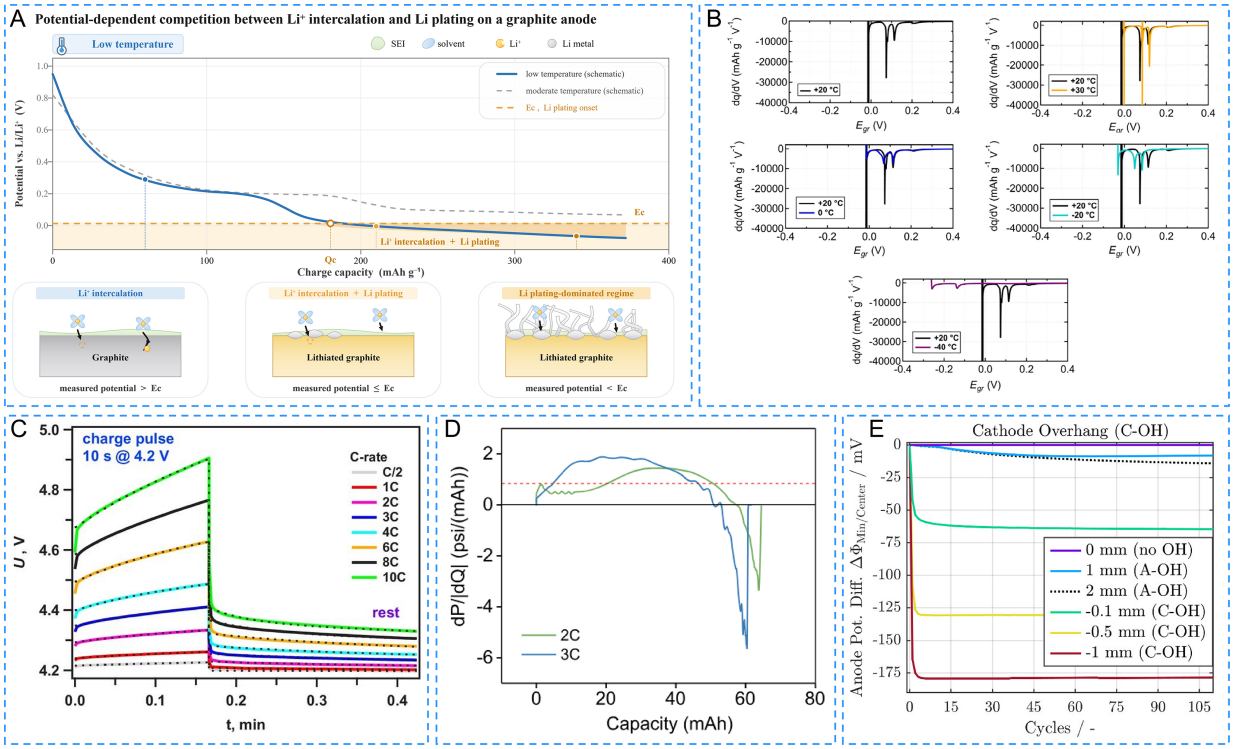


Figure 4. (A) Schematic illustration of the potential dependent competition between Li^+ intercalation and lithium plating on a graphite anode during galvanostatic charging of a lithium-ion battery at low temperature. (B) Differential capacity analysis of the graphite electrode potential, E_{gr}, in the three-electrode Li, Li, graphite cell, (B) Reproduced from Ref.[64], licensed under CC BY 4.0. (C) Transient full-cell voltage responses to 10 s charging pulses at different C-rates; (C) Reproduced from Ref.[66], licensed under CC BY 4.0. (D) Differential-pressure profiles (d_P/d_Q) of graphite/NMC532 pouch cells charged at 2 and 3 C, illustrating the rate-dependent onset of lithium plating; (D) Reproduced from Ref.[69], licensed under CC BY 4.0. (E) Calculated differences between local anode-edge and central potentials for different electrode overhang configurations during cycling; (E) Reproduced from Ref.[73], licensed under CC BY 4.0.

dominant reaction pathway under low-temperature conditions [Figure 4B].

Kinetic analysis further showed that Li^+ intercalation deviated from conventional Arrhenius behavior. Li^+ was first reversibly adsorbed on the graphite surface, followed by charge transfer leading to the formation of LiC_6 or metallic lithium. By contrast, lithium plating followed typical Arrhenius behavior, indicating a single-step unimolecular process. Mao *et al.*[65] systematically examined the combined effects of low temperature and current rate on lithium plating through electrochemical measurements, materials characterization, and numerical analysis. As the temperature decreased and the charging rate increased, the dominant charging mechanism gradually shifted from conventional lithium intercalation to lithium plating. At -20 °C and a charging rate of 0.5 C, the cell ultimately failed completely.

Lithium plating induced by fast charging

High-rate charging is another major factor promoting lithium plating on graphite anodes. At high current densities, the flux of Li^+ delivered to the graphite/electrolyte interface increases substantially. When Li^+ transport through the electrolyte and SEI, interfacial charge transfer, and subsequent solid-state diffusion within graphite cannot accommodate the imposed ion flux, Li^+ accumulates near the electrode surface, progressively increasing the local overpotential and favoring metallic lithium deposition over intercalation into the graphite lattice[6]. Shkrob *et al.*[66] investigated cell polarization during rapid charging through charge-pulse and voltage-relaxation experiments at different rates. As shown in Figure 4C, when 10 s charging pulses were applied to an NCM523/graphite full cell initially equilibrated at 4.2 V, increasing the rate from 0.5 to 10 C markedly increased both the voltage rise during charging and the immediate voltage

drop upon current interruption, followed by gradual voltage relaxation. Separate anode-potential measurements further showed that high-rate pulses could drive the graphite anode potential below 0 V *vs.* Li^+/Li, bringing the anode into a potential regime where lithium plating becomes possible. Colclasure *et al.*[67] developed an electrochemical model validated with cells of different electrode loadings. The model showed that poor electrolyte transport limits the performance of high-energy-density cells, leading to salt depletion in the anode and lithium plating at the graphite separator interface. Potential analysis further indicated that restricted liquid-phase transport increases local polarization, causing this interface to reach the conditions for metallic lithium deposition earlier than other regions.

Lithium plating generally begins as graphite approaches lithium intercalation saturation, and its onset occurs at an earlier stage of charging as the charging rate rises[68]. Huang *et al.*[69] employed operando differential pressure sensing to investigate lithium plating in graphite/NMC532 pouch cells during fast charging. As shown in Figure 4D, the pressure change per unit charge (d_P/d_Q) at both 2 and 3 C exceeded the lithium-plating threshold established under low-rate lithium intercalation conditions. Compared with 2 C, the 3 C profile crossed this threshold at a lower charge capacity and exhibited a higher maximum, indicating that increasing the charging rate accelerated the onset of lithium plating and intensified metallic lithium deposition. The negative values near the end of charging were associated with a pressure decrease caused by the reintercalation of plated lithium into graphite as the current declined during the constant-voltage stage. In addition, the relationship between interfacial charge-transfer resistance and state of charge exhibits pronounced rate dependence. A separate study reported that lithium plating began at a lower state of charge as the charging rate increased. In that cell system, lithium nucleation was already observed during 3 C charging at room temperature, whereas increasing the rate from 4 to 6 C intensified metallic lithium deposition and promoted the development of dendritic morphologies[70].

Cell design defects

Cell design defects are another important reason for lithium loss. An excessively low N/P ratio (the ratio of the anode capacity to the cathode capacity) indicates insufficient negative electrode capacity relative to the positive electrode, causing graphite to approach full lithiation more readily during charging and thereby increasing the risk of lithium plating. Abe *et al.*[71] investigated the influence of the ratio of anode and cathode electrode capacities on the charging-discharging rate capability and cycle performance of $LiFePO_4$/graphite LIBs. The results showed that cells with a lower N/P ratio exhibit stronger polarization phenomena, which is related to a decrease in specific capacity.

The ratio of the anode and cathode areas also affects the deposition of lithium. Kim *et al.*[72] investigated the lithium deposition near the electrode edges when the N/P ratio was relatively low. They compared three electrode configurations: an anode area larger than the cathode area, a cathode area larger than the anode area, and equal anode and cathode areas. At all test rates, the battery with a cathode area larger than the anode area exhibited the highest amount of lithium metal deposition. This result indicates that insufficient anode coverage leads to the accumulation of Li^+ flux near the electrode edges, thereby promoting lithium deposition. In contrast, when the electrode area is equal or the anode area is larger than the cathode area, the amount of lithium deposition is significantly reduced. Extending the anode beyond the cathode was more effective in suppressing lithium plating at higher charging rates. Roth *et al.*[73] further investigated the influence of electrode misalignment on the local anode potential distribution using a two-dimensional electrochemical model. As shown in Figure 4E, cathode overhangs of 0.1, 0.5, and 1 mm produced decreases in the anode-edge potential exceeding 60, 125, and 175 mV relative to the center after the first cycle, indicating a substantially increased risk of edge plating. In contrast, perfectly aligned electrodes maintained a nearly zero potential difference in this model. Although anode overhang also induced local potential heterogeneity during continuous cycling, its magnitude was considerably smaller than that caused by

cathode overhang. These results indicate that anode overhang helps mitigate severe edge effects arising from manufacturing-induced misalignment, while its contribution to cycling-induced lithiation heterogeneity should also be considered in cell design.

Manufacturing defects, including active material detachment near electrode edges, nonuniform calendering, and their combined occurrence, can markedly alter the internal electrochemical environment and increase the risk of lithium plating. Chen *et al*.[74] developed several three-dimensional electrochemical models to systematically clarify the effects of these electrode manufacturing defects. The models separately evaluated active material detachment near the anode edge caused by coating defects, density nonuniformity caused by uneven calendering in the electrode edge region, and the combined effects of both defects. In addition to promoting lithium plating, these defects may accelerate the formation of inactive lithium, repeated SEI reformation, and interfacial side reactions, ultimately intensifying capacity decay and increasing safety risks. Each of these factors can lower the local anode potential into the lithium plating region, thereby increasing the likelihood of metallic lithium deposition.

Mechanical damage to the graphite structure

Mechanical damage to graphite anodes originates primarily from the volume changes and progressive stress accumulation during cycling[75]. From a mechanical perspective, graphite particles expand during the lithiation process and contract during the delithiation process. This periodic change in volume generates diffusion-induced stress within the particles and in the electrode coating[76]. As shown in Figure 5A and B, the strain response of the graphite anode significantly changes with the variation of lithium concentration and the number of cycles, reflecting the continuous evolution of internal stress during the repeated lithiation and delithiation processes. When the local stress reaches a sufficiently high level, microcracks may form within the graphite particles and expand as the cycles continue. Clear internal cracks can be observed in the graphite particles after the cyclic treatment, and their expansion within the particles highlights the mechanical damage caused by repeated lithium insertion and extraction[42]. Such cracks may eventually lead to particle pulverization, weakening the electronic contact of the active material, and exposing the originally buried graphite surface to the electrolyte These newly exposed surfaces subsequently undergo the formation of SEI films and electrolyte decomposition, which consume the active lithium, gradually increasing the cell impedance and resulting in the observed capacity loss.

Fracture and pulverization of active particles

Fracture and pulverization are the typical mechanical failure modes of active particles in graphite anodes[77]. Both arise from volume changes and diffusion-induced stresses, which build up during repeated cycling[78]. Because Li^+ transport and phase changes are not uniform across the particle, the stress distribution is also heterogeneous. Local stress concentrations therefore tend to develop around grain boundaries, particle edges and corners. The maximum tensile stress increases significantly with increasing charge rate and decreasing temperature. Under these aggressive operating conditions, local stress can easily exceed graphite's tensile strength, and that's when cracks start[79]. Once a crack appears, further cycling makes it grow and join up with nearby cracks, eventually breaking the particle apart [Figure 5C][80].

These processes disrupt the structural framework of the graphite electrode and can also break electrical pathways between active particles and the conductive network. Fractured material loses effective electrochemical contact, leading to irreversible capacity loss[81]. More importantly, fracture creates fresh graphite surfaces that are no longer protected by the existing SEI. These exposed surfaces induce further electrolyte reduction and SEI formation[82]. This triggers continuous SEI reconstruction, a parasitic process that irreversibly depletes active lithium and electrolyte. Concurrently, the accumulating interphase thickens the diffusion barrier, leading to a steady rise in interfacial resistance.

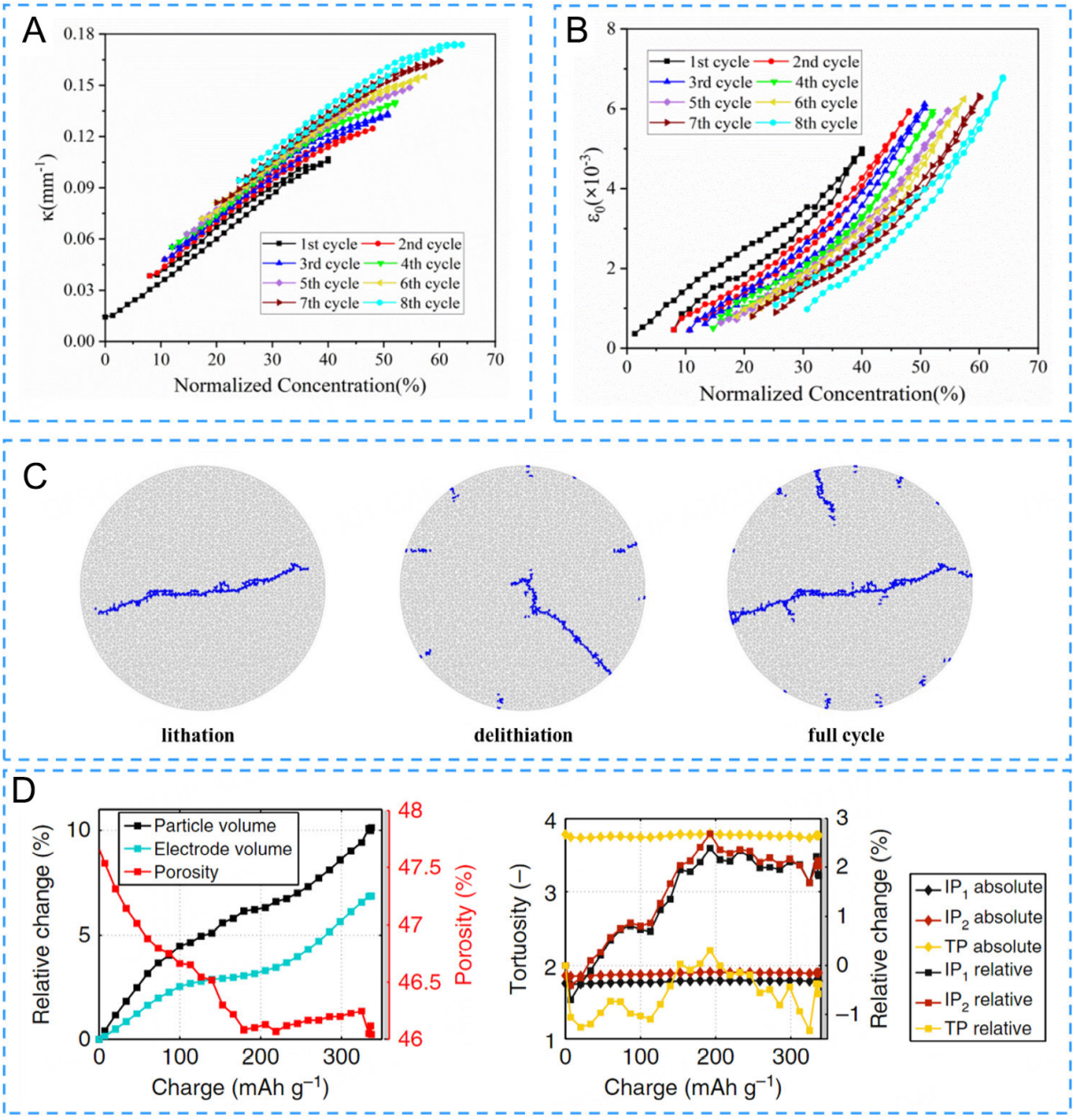


Figure 5. (A) Evolution of graphite-electrode bending curvature and (B) in-plane strain with normalized lithium concentration over repeated cycles; (A and B) Reproduced from Ref.[76], licensed under CC BY 4.0. (C) Crack patterns; (C) Reproduced from Ref.[80], licensed under CC BY 4.0. (D) Changes in dynamic volume, porosity, and tortuosity; (D) Reproduced from Ref.[84], licensed under CC BY 4.0.

Degradation of the electrode architecture

Mechanical damage of graphite particles can gradually affect the overall anode structure. Due to the expansion and cracking, the transport pathways become increasingly heterogeneous[83]. As shown in Figure 5D, both the particle and electrode volumes vary considerably during charging, together with changes in porosity and directional tortuosity[84]. The pore network can also influence the electrolyte access and Li^+ transport. Although the generated voids provide additional space for electrolyte penetration, excessive cracking and particle rearrangement can simultaneously reduce the solid-phase contacts. The resulting transport heterogeneity can produce local variations in current density and increase electrode polarization[85].

Intrinsic defects in the graphite lattice

Defects in the graphite lattice can also influence the mechanical instability at the atomic scale. The typical defects include Stone-Wales defects, single vacancies, and divacancies. By changing the local sp^2 carbon network, these defects reduce the mechanical integrity of the lattice and lower both the Young's modulus and ultimate tensile strength of graphite. During cycling, defect-rich regions tend to experience greater local strain and are more prone to fracture than their well-ordered counterparts[86]. These defects can also act as hotspots for stress buildup, making them natural nucleation sites for microcracks that can subsequently propagate through the graphite particle[87]. As cycling proceeds, these defects may become localized structural instabilities and form larger cracks and particle fragmentation. This degradation pathway directly undermines both the structural integrity of the electrode and its ability to retain capacity over extended operation[88].

Coupled failure mechanisms of graphite anodes

SEI instability, lithium plating, and mechanical degradation in graphite anodes are closely interconnected during cycling rather than being isolated failure processes. Repeated lithiation and delithiation cause the graphite particles to expand and contract, generating local mechanical stress that can eventually promote particle cracking and damage the surrounding SEI. Exposure of fresh graphite then triggers further electrolyte reduction and SEI regrowth. In addition to consuming active lithium and electrolyte, repeated SEI formation gradually increases the thickness and resistance of the interphase, which hinders Li^+ transport and contributes to greater electrode polarization[89]. With continued cycling, particle rearrangement, pore-structure changes, and the loss of electronic contact can further disturb Li^+ transport and current distribution across the electrode. These effects become more pronounced at high electrode loading or under nonuniform mechanical constraints, where local differences in transport and stress can develop within the electrode. Such local heterogeneity is particularly important under fast-charging, low-temperature, or high-states of charge (SOC) conditions, as regions with poor transport or high polarization may reach potentials favorable for lithium plating. Once metallic lithium is deposited, it can react with the electrolyte and generate additional interphase products, while part of the deposited lithium may become electrochemically inactive. The newly formed interphase and deposited lithium can also alter the local structure and transport environment, creating further conditions for SEI damage, plating, and particle degradation. Through repeated cycling, these processes can therefore spread from localized defects at the particle surface to larger regions of the electrode. The resulting accumulation of inactive lithium, rising interfacial and charge-transfer resistance, and progressive structural damage ultimately contribute to capacity loss and increasing safety concerns.

STRUCTURAL AND INTERFACIAL OPTIMIZATION OF GRAPHITE ANODES

Optimization of graphite materials

The performance of graphite anodes is closely related to their particle morphology, crystal structure, pore network, and surface chemistry. These characteristics affect Li^+ transport and interface reactions, thereby influencing the cycling stability of the electrode. Therefore, modifying graphite is an important approach to suppress lithium plating, side reactions, and mechanical damage during the cycling process[90]. Current research methods mainly focus on three aspects: applying carbon coatings to the particle surface, regulating the interlayer structure of graphite, and introducing heteroatom dopants. These modification methods are intended to stabilize the electrode-electrolyte interface, improve Li^+ transport, and enhance the graphite structure. However, their effectiveness depends on the degree of coating, structural regulation, and doping, while excessive modification may hinder Li^+ transport; these strategies are therefore more suitable for graphite systems limited by interfacial instability or sluggish ion transport.

Carbon coating

Amorphous carbon coating has been widely used to improve the interfacial stability and electrochemical kinetics. A carbon layer on the graphite surface can limit the direct exposure of highly reactive sites to the electrolyte, which is beneficial for the suppression of side reactions. The carbon coating can also accommodate the volume changes of graphite during cycling. Meanwhile, the coating modifies the subsequent formation of the SEI, favoring a more uniform interphase and lowering interfacial resistance. These effects can significantly improve the electrochemical performance. Xiao *et al.*[91] prepared amorphous carbon-coated graphite (GC) by chemical vapor deposition. As shown in Figure 6A, cross-sectional scanning electron microscopy of GC-2, obtained after 2 h of deposition, revealed a carbon coating approximately 90 nm thick, with local thicknesses of 89.3 and 91.8 nm at the two indicated positions. This coating covered unstable structures on the graphite surface, limiting their direct contact with the electrolyte. Meanwhile, the carbon layer provided additional pathways for Li^+ diffusion, improved interfacial reaction kinetics, and reduced electrode polarization, thereby mitigating the risk of lithium plating during fast charging. The pouch cell assembled with a GC-2 anode and a $LiCoO_2$ cathode retained 87% of its initial capacity after 1,200 cycles at a charge/discharge rate of 5 C/5 C, demonstrating stable cycling performance at high rates [Figure 6B]. Ma *et al.*[92] developed a Zn/N co-doped amorphous carbon coating on graphite through the *in situ* growth of ZIF-8 followed by carbonization. It exhibited enlarged interlayer spacing and enhanced lithiophilicity, which facilitated Li^+ transport and promoted uniform lithium deposition/intercalation. Defects introduced by edge nitrogen doping provided rapid diffusion channels for Li^+ between the carbon layers.

Regulation of interlayer spacing

Zhang *et al.*[93] proposed a scalable interlayer spacing regulation process that integrates mild oxidative intercalation with thermal reduction to enlarge the graphite interlayer spacing while repairing structural defects introduced during oxidation. Using this strategy, low-defect expanded graphitized needle coke was successfully synthesized. After modification, the densely stacked layers of petroleum coke-derived graphite became more open, giving rise to an expanded graphite structure. The interlayer spacing increased from 0.3375 to 0.3427 nm, while the graphite lattice was largely retained. This structural optimization enabled enhanced ion-accessible pathways without causing the severe lattice disruption typically associated with conventional strong acid oxidation treatments. A moderate increase in interlayer spacing can improve Li^+ transport within graphite. Zha *et al.*[94] prepared CO_2-derived graphite with expanded interlayer spacing (NK-M_4) by coupling molten-salt electrolysis of dilute CO_2 with *in situ* alkali-metal exfoliation. The volumetric expansion and shear forces associated with the *in situ* generated alkali metals promoted the expansion of graphite interlayers. As shown in Figure 6C, the interlayer spacing in the bulk region predominantly ranged from 0.338 to 0.341 nm, whereas local spacings near the edge increased to 0.352 and 0.364 nm. Figure 6D further reveals local edge spacings of 0.381 and 0.405 nm alongside clearly resolved graphite lattice fringes, demonstrating the coexistence of an ordered layered structure and localized interlayer expansion at the edges. Electrochemical measurements further indicated that this interlayer expansion facilitated Li^+ diffusion and reduced charge-transfer resistance, thereby enhancing the high-rate lithium-storage performance of graphite. Rathi *et al.*[95] reported a bifunctional acid treatment strategy for graphite modification. This approach simultaneously enlarged the graphite interlayer spacing and introduced nanopores, thereby shortening Li^+ diffusion pathways and improving electrode reaction kinetics. As shown in Figure 6E, the treated expanded porous graphite (EG) exhibited a larger interlayer spacing and a more developed pore structure than pristine graphite (PG), while retaining the structural integrity of the graphite framework. The combined expansion of interlayer spacing and formation of nanopores accelerated Li^+ intercalation and deintercalation, reduced diffusion resistance and polarization, and consequently improved rate capability and cycling stability. Based on the single-layer spacing regulation, Liu *et al.*[96] further proposed a surface-embedded phase collaborative regulation strategy, and prepared ultrathin disordered carbon-coated micro-expanded graphite. The gentle intercalation and thermal expansion increased the graphite layer spacing from

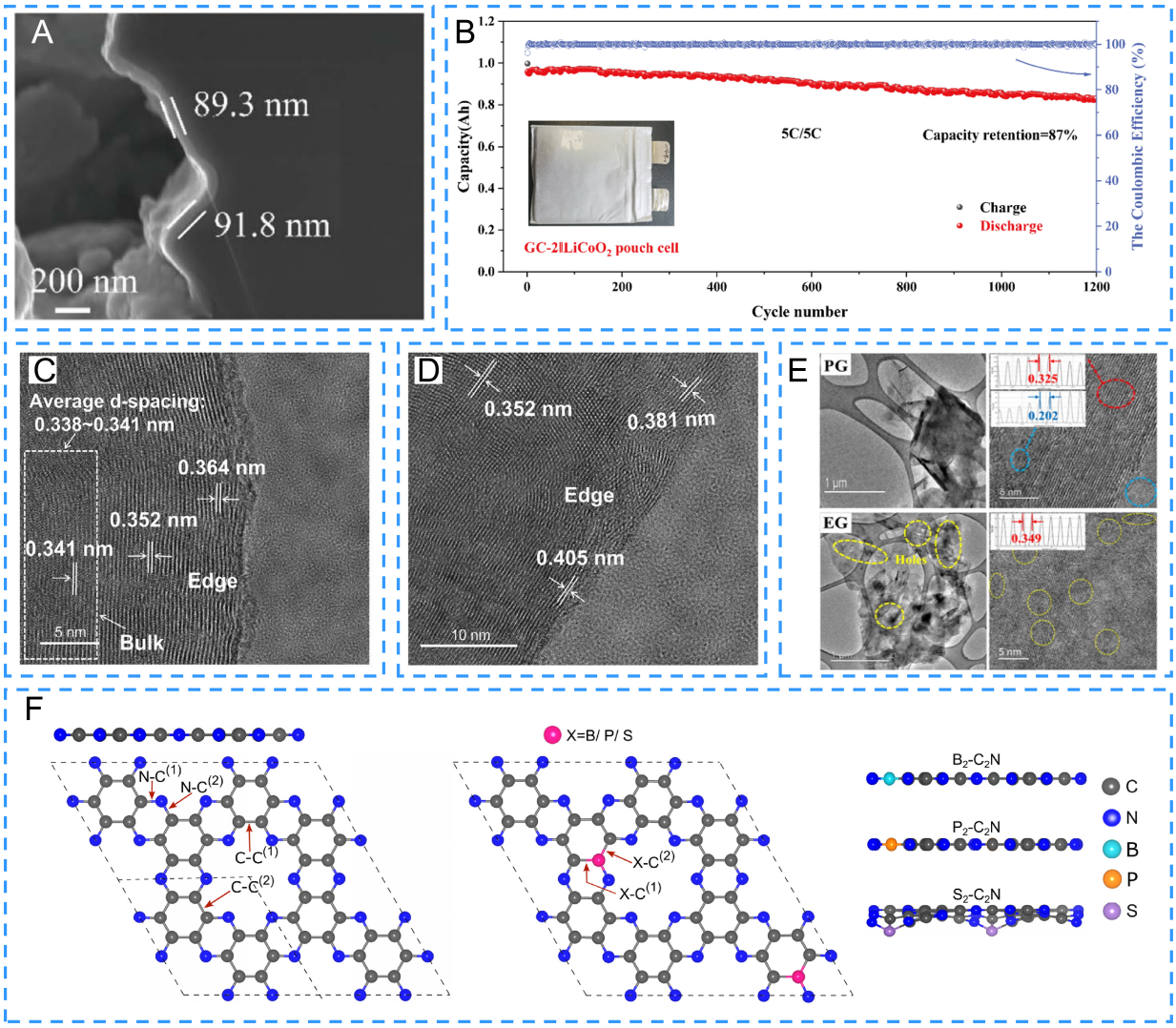


Figure 6. (A) Cross-sectional scanning electron microscopy image of the amorphous carbon coating on GC-2 graphite, showing local coating thicknesses of approximately 90 nm, (B) Cycling performance of GC-2 at 5 C, (A and B) Reproduced from Ref.[91], licensed under CC BY-NC 3.0. (C and D) High-resolution transmission electron microscopy images revealing locally expanded graphite interlayer spacings, particularly near the edges, in CO_2-derived expanded graphite, (C and D) Reproduced from Ref.[94], licensed under CC BY 4.0. (E) HRTEM images of pristine PG and EG, (E) Reproduced from Ref.[95], licensed under CC BY-NC 3.0. (F) Top- and side-view atomic structures of pristine C_2N and B-, P-, or S-substituted C_2N monolayers, illustrating dopant-dependent structural distortion, (F) Reproduced from Ref.[97], licensed under CC BY 4.0.

approximately 0.335 to 0.338 nm, forming more open edge lithium-intercalation channels; the approximately 5 nm disordered carbon layer on the surface provided defect adsorption sites and pseudocapacitive lithium storage behavior, while also improving the Li^+ transport between particles and the interface compatibility between the electrode and the electrolyte. This combined regulation reduced the interface impedance and electrode polarization, promoted the formation of a thin and uniform inorganic-enriched SEI, and alleviated lithium shedding and particle cracking under high current density.

Elemental doping

Elemental doping can modify the electronic structure and local chemical environment of graphite, which in turn affects Li^+ adsorption, diffusion, and interfacial reactions. In a related two-dimensional carbon-based system, Ghorbani Shadpey *et al.*[97] used first-principles calculations to investigate the effects of B, P, and S substitutional doping on the structure and lithium-storage behavior of porous C_2N monolayers. As shown in

Figure 6F, substitution of carbon sites with heteroatoms produced X_2-C_2N structures (X = B, P, or S). The B- and P-doped systems remained largely planar, whereas S doping induced pronounced out-of-plane buckling, reflecting dopant-dependent changes in local bonding and lattice deformation. Further calculations showed that strong Li binding near B dopants created deep potential wells that hindered diffusion, whereas the local Li migration barrier near S dopants was approximately 0.36 eV. These results highlight the need to balance Li adsorption strength with ion-migration kinetics when designing heteroatom-doped structures, thereby avoiding excessively strong local binding that restricts Li diffusion. Huo *et al.*[98] explored a bilayer graphene model and first-principles calculations to examine how nitrogen defects on graphite basal planes affect lithium nucleation and deposition. Introducing single-vacancy nitrogen defects (SV-3N) and divacancy nitrogen defects (DV-4N) changes the local electronic structure of the basal plane and increases its lithium affinity. Lithium preferentially adsorbs and deposits around the defective sites under an applied electric field. The SV-3N and DV-4N defects provide distributed nucleation sites, which helps to reduce local lithium accumulation and promotes a more even deposition process. The calculations further showed that nitrogen defects can regulate lithium adsorption energies, diffusion pathways, and lithiation behavior, providing a possible route to suppress heterogeneous lithium nucleation. Furthermore, other carbon-based electrode systems have also shown that the high electronegativity of nitrogen can redistribute electron density, while different nitrogen configurations exhibit distinct electronic structures and interfacial reactivities[99].

Electrolyte and interfacial engineering

Electrolyte engineering provides a direct method of regulating the interfacial chemistry and ion-transport kinetics of graphite anodes. Beyond serving as the medium for Li^+ transport, the electrolyte determines the solvation environment of Li^+, the kinetics of desolvation and interfacial charge transfer, and the composition and structure of the resulting SEI[15]. Accordingly, electrolyte optimization can mitigate several key degradation pathways identified above, including excessive SEI growth, solvent cointercalation, interfacial polarization, and lithium plating. Current strategies can be categorized into electrolyte composition and salt engineering, solvation structure engineering, and artificial interphase engineering, which progressively regulate the bulk electrolyte, the local Li^+ solvation environment, and the electrode/electrolyte interface, respectively. However, their effectiveness is constrained by electrolyte composition, operating temperature, and electrochemical stability window, making these strategies more suitable for systems limited by interfacial side reactions or sluggish Li^+ transport kinetics.

Electrolyte composition and salt engineering

Modification of electrolyte composition and lithium salt chemistry represents a straightforward approach to regulating SEI formation and interfacial transport. By introducing functional ionic species or adjusting the salt composition, the reduction pathways of electrolyte components can be redirected toward the formation of more stable interphases, while ionic conductivity and low-temperature interfacial kinetics can also be improved. Wang *et al.*[100] developed a multisalt high-entropy (HE) electrolyte by combining equimolar $LiPF_6$, LiTFSI, LiFSI, LiDFOB, and $LiNO_3$ in PC, each at 0.2 M, giving a total salt concentration of 1.0 M. As illustrated in Figure 7A, increasing the diversity of lithium salts enhanced anion participation in Li^+ solvation and weakened Li^+-PC interactions, producing an anion-rich, disordered solvation sheath and promoting the formation of an inorganic-rich SEI dominated by salt decomposition. During the initial discharge at 0.1 C, the HE electrolyte exhibited a short plateau at approximately 1.7 V *vs.* Li^+/Li, while effectively suppressing the prolonged plateau near 0.7 V associated with solvent cointercalation in the single-salt PC electrolytes. The potential subsequently decreased into the low-potential regime for lithium intercalation into graphite. These results demonstrate that varying salt composition, rather than increasing the total salt concentration, can jointly regulate solvation chemistry and interphase formation, suppressing PC cointercalation and improving compatibility with graphite anodes. Luo *et al.*[101] introduced four representative SEI components, LiF, $LiNO_3$, Li_2O, and Li_2CO_3, into a commercial electrolyte to construct a multicomponent solute high-entropy

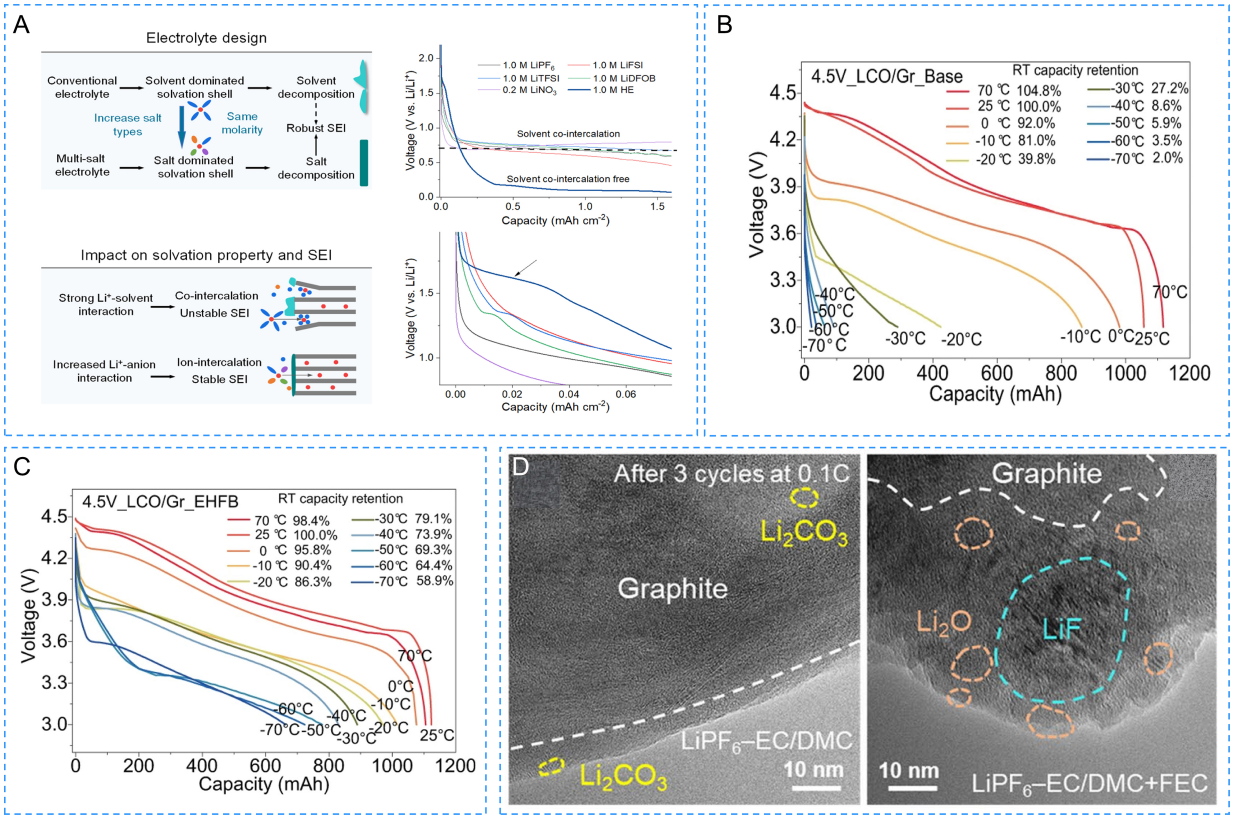


Figure 7. (A) Design concept of a multisalt high-entropy electrolyte, its influence on Li^+ solvation and SEI formation, and initial graphite discharge profiles in different propylene carbonate-based electrolytes; (A) Reproduced from Ref.[100], licensed under CC BY 4.0. Temperature-dependent discharge curves of $LiCoO_2$/graphite pouch cells with (B) the baseline electrolyte and (C) the ethyl heptafluorobutyrate (EHFB)-containing electrolyte; (B and C) Reproduced from Ref.[106], licensed under CC BY 4.0. (D) High-resolution transmission electron microscopy images comparing SEI microstructures formed on graphite in $LiPF_6$-EC/DMC without and with fluoroethylene carbonate (FEC); (D) Reproduced from Ref.[108], licensed under CC BY 4.0.

electrolyte. The modified electrolyte maintained excellent rate performance even at low temperatures. This improvement was attributed to the combined effects of a weakly solvated Li^+ environment and reduced interfacial activation energy, facilitating the Li^+ transport across the electrode/electrolyte interface. The type of lithium salt also has a significant impact on the low-temperature interface dynamics. Raj *et al.*[102] compared the electrochemical performance of $LiPF_6$, $LiBF_4$, and LiDFOB electrolyte salts with graphite anodes over a temperature range from -30 to 25 °C. The specific capacity of all electrolyte systems decreased as the temperature decreased, whereas the LiDFOB-based electrolyte (PEC113) exhibited the highest capacity retention and showed the lowest resistance at -30 °C, indicating more favorable ionic transport and interfacial charge-transfer kinetics.

Solvation structure engineering

While electrolyte composition determines the chemical environment from which the SEI forms, the local solvation structure of Li^+ directly governs its desolvation and subsequent transfer across the electrode/electrolyte interface. In particular, excessive solvent coordination can increase the desolvation barrier and promote solvent-related side reactions, whereas weakly solvating environments can facilitate interfacial Li^+ transport and suppress undesirable solvent participation. Solvation structure engineering has therefore emerged as an effective strategy for improving both fast-charging capability and low-temperature performance. Zheng *et al.*[103] developed a weakly solvating electrolyte for fast-charging graphite anodes by introducing methyl acetate and fluorinated ethyl methyl carbonate (FEMC), both of which exhibit relatively

weak Li^+-solvent interactions. The FEMC-based electrolyte contained a larger fraction of anion-rich aggregates than the conventional EMC-based electrolyte. The modified solvation structure lowered the Li^+ desolvation barrier and interfacial resistance, which favored faster charge transfer during high-rate charging. The corresponding SEI was also richer in inorganic components, with LiF becoming the dominant species. In the 1 M LiFSI/FEMC electrolyte, the LiF content reached about 90%, providing a more stable interface and facilitating Li^+ transport across the interphase. Graphite electrodes in this weakly solvating electrolyte consequently delivered better rate performance and maintained relatively high discharge capacities at 2 and 4 C.

Beyond solvation structure, the size and spatial distribution of LiF within the SEI also significantly influence interfacial transport. Tao *et al.*[104] investigated the influence of SEI microstructure on graphite anode kinetics using a weakly solvating electrolyte of 1 M $LiPF_6$ in 2-methyltetrahydrofuran (2MeTHF). Li^+ insertion involves bulk transport, interfacial desolvation, transport across the SEI, and diffusion within graphite. The $LiPF_6$-2MeTHF electrolyte exhibited a contact-ion-pair-dominated solvation structure and formed an SEI with small, dispersed LiF crystallites, enabling effective passivation and favorable Li^+ transport. In contrast, adding 2 vol.% FEC or replacing $LiPF_6$ with LiFSI generated larger, more densely distributed LiF crystallites, increasing SEI transport resistance. Despite similar desolvation barriers, these electrolytes showed substantially different activation energies for Li^+ transport through the SEI, highlighting the importance of SEI microstructure. At -20 °C and 0.2 C, the $LiPF_6$-2MeTHF electrolyte maintained high reversible capacity. After rate testing, the cell retained approximately 91% capacity by the 200th test cycle at 2 C and 23 °C, with an average Coulombic efficiency of 99.9%. These findings demonstrate that coordinated control of solvation and SEI microstructure can improve fast-charging and low-temperature performance.

For operation over a broader temperature range, Luo *et al.*[105] introduced isobutyronitrile (iBN) as a cosolvent to develop an electrolyte with a broad operating temperature range. Its low viscosity, relatively high dielectric constant, and weak coordination with Li^+ weakened Li^+-solvent interactions and lowered the desolvation energy barrier. The electrolyte maintained relatively high ionic conductivity as the temperature decreased, helping to reduce transport and interfacial kinetic losses. A $LiCoO_2$/graphite pouch cell using the iBN-60 electrolyte still delivered a relatively high discharge capacity at -70 °C. These results suggest that tuning Li^+ solvation can be useful at both high and low temperatures, where desolvation and ion-transport kinetics become important limitations for graphite-based cells. Chen *et al.*[106] introduced ethyl heptafluorobutyrate (EHFB) as a fluorinated cosolvent to regulate the Li^+ solvation structure, shifting it from EC -dominated to diethyl carbonate-dominated coordination. This modification weakened Li^+-solvent interactions, facilitated Li^+ desolvation, and promoted the formation of a LiF-rich SEI on graphite. As shown in Figure 7B, the $LiCoO_2$/graphite pouch cell with the baseline electrolyte exhibited severe capacity decay at low temperatures, retaining only 8.6% and 2.0% of its room-temperature discharge capacity at -40 and -70 °C, respectively. In contrast, the EHFB-containing electrolyte significantly improved capacity retention to 73.9% and 58.9% at the corresponding temperatures [Figure 7C]. These results demonstrate that optimizing the solvation structure and interfacial chemistry can effectively improve the low-temperature performance of graphite-based batteries.

Artificial interphase and electrolyte-derived interfacial engineering

The effects of electrolyte regulation are closely reflected at the electrode/electrolyte interface, where the SEI controls Li^+ transport, electron transfer, and parasitic reactions. Artificial interphase engineering offers an alternative to the SEI formed solely through electrolyte decomposition by allowing its composition, structure, and transport properties to be tailored in advance. Such strategies can provide more uniform Li^+ transport, suppress continuous electrolyte reduction, and mitigate the interfacial polarization associated with fast charging. Liu *et al.*[107] constructed a graphite-muconic acid composite anode (Gra@MCA) through an *in situ*

synthesis strategy, in which the muconic acid (MCA) layer served as a rechargeable organic artificial SEI. Compared with the conventional SEI, which can exhibit heterogeneous ion-transport pathways and increased interfacial resistance under high-rate conditions, the MCA layer provided more continuous and uniform pathways for Li^+ transport. This regulated interfacial environment promoted more homogeneous lithiation, reduced anode polarization, and lowered interfacial resistance. Consequently, the Gra@MCA electrode exhibited substantially improved rate capability and cycling stability compared with PG. Weng *et al.*[108] introduced 10 vol.% FEC into a $LiPF_6$-EC/dimethyl carbonate (DMC) electrolyte to regulate SEI composition and interfacial transport kinetics on graphite anodes. As shown in Figure 7D, the SEI formed in the conventional electrolyte consisted mainly of amorphous organic species and Li_2CO_3 nanograins, with a thickness of approximately 3-7 nm. In contrast, FEC addition produced an SEI containing LiF nanoparticles, Li_2O nanograins, and amorphous organic components, resulting in a distinct interfacial microstructure. Despite its increased thickness of 44-56 nm, the modified SEI exhibited a reduced ion-transport resistance from 13.77 to 4.67 Ω, indicating improved Li^+ transport across the interphase. Consequently, the reversible capacity of graphite at 4 C increased from 62.0 to 276.2 mAh g^{-1}, demonstrating enhanced high-rate lithium-storage performance. Studies of other carbon-based electrode systems have shown that the higher electronegativity of nitrogen atoms can redistribute the electron density within the carbon framework, while different types of nitrogen sites may exhibit distinct interfacial reactivities[109]. More sophisticated interfacial architectures can further integrate the functions of electronic conduction, Li^+ transport, and mechanical protection.

Electrode structure design

The performance of graphite anodes is not only determined by the inherent properties of the graphite particles and the chemistry of the electrode/electrolyte interface, but also influenced by the mesoscale structure in the composite electrode. During cycling, particle expansion, pore restructuring, electrolyte redistribution, and loss of electronic contact continuously alter the coupled ion and electron transport networks. These effects are more pronounced in thick and high-loading electrodes. Due to the longer transmission distance of Li^+ and the uneven current distribution in these electrodes, these factors can intensify concentration polarization and increase the likelihood of lithium precipitation. Therefore, the electrode structure design aims to coordinate the pore structure, the connectivity between particles, mechanical integrity, and the transport of ions/electrons across multiple length scales. Current strategies can be broadly classified into pore-structure engineering, binder and interparticle mechanical engineering, and three-dimensional conductive or gradient electrode structures. These strategies require a balance between transport enhancement and structural complexity, and are particularly suitable for thick and high-loading electrodes limited by ion/electron transport.

Pore structure design

Pore architecture plays a central role in determining electrolyte penetration, Li^+ transport, and the distribution of local current within graphite electrodes. Therefore, rational adjustment of pore size, connectivity, tortuosity, and spatial distribution is an important way to improve ion transport and reduce local Li accumulation. Ahmadi *et al.*[110] investigated the effects of electrode microstructure on Li^+ transport and cycling stability by constructing particle-size-gradient (PSG) and PG graphite anodes. As illustrated in Figure 8A, unlike conventional electrodes with a uniform microstructure, the PSG electrodes featured progressively larger graphite particles from the current collector toward the separator, whereas the PG electrode exhibited a gradual increase in porosity from 24% near the current collector to 46% near the separator. These gradient structures improved Li^+ transport across the electrode thickness and reduced local concentration gradients and charge-transfer resistance, thereby alleviating electrode polarization. As shown in Figure 8B, after 200 cycles at room temperature with lithiation at 2 C and delithiation at C/3, the PG electrode retained approximately 80% of its initial capacity, outperforming PSG1 (67%), PSG2 (60%), and the

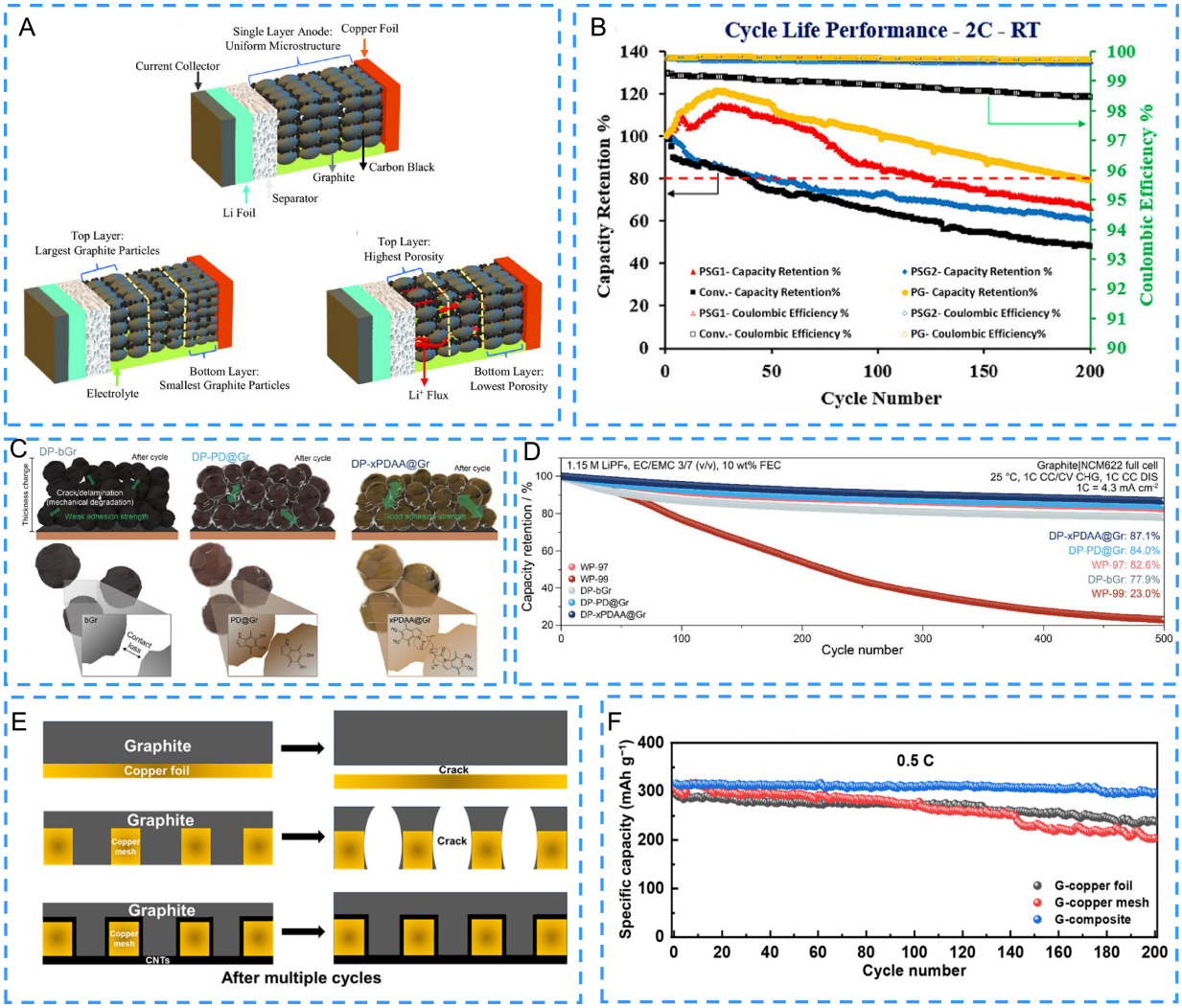


Figure 8. (A) Schematic comparison of a conventional graphite electrode, a particle-size-gradient (PSG) electrode, and a porosity-gradient (PG) electrode, (B) Capacity retention and Coulombic efficiency of conventional, PSG, and PG graphite electrodes during cycling at 2 C and room temperature; (A and B) Reproduced from Ref.[110], licensed under CC BY 4.0. (C) Schematic comparison of particle contact and mechanical integrity in dry-processed bare graphite (DP-bGr), polydopamine-coated graphite (DP-PD@Gr), and crosslinked graphite (DP-xPDAA@Gr) electrodes, (D) Cycling stability of graphite/NCM622 full cells fabricated using these electrodes; (C and D) Reproduced from Ref.[114], licensed under CC BY 4.0. (E) Schematic of graphite-electrode cracking and interfacial contact loss on copper foil, copper mesh, and carbon nanotube (CNT)-coated copper mesh current collectors, (F) Cycling performance of graphite electrodes using the three current collectors at 0.5 C; (E and F) Reproduced from Ref.[116], licensed under CC BY 4.0.

conventional electrode (47%). The gradient electrodes also maintained Coulombic efficiencies above 99%, demonstrating that optimizing particle size and pore distribution can improve graphite-anode reaction kinetics and mitigate capacity degradation.

In conventional graphite electrodes, the pressing process causes the particles to be densely packed and compresses the pore network, thereby confining Li^+ transport pathways and promoting local polarization and surface lithium plating during high-rate charging. By contrast, introducing through-hole carbon spheres (THCS) can create a gradient pore structure and interconnected transmission network within the electrode. As a result, Li^+ can penetrate more effectively from the surface into deeper regions of the electrode, thereby reducing local concentration gradients and lowering the likelihood of lithium deposition. Electrochemical measurements further confirmed the effectiveness of this structural design. Under different charging rates, the THCS electrode delivered higher capacity and exhibited lower polarization, demonstrating significantly

improved ion transport kinetics. However, merely optimizing the pore structure may still result in local current concentration in the channel region. Therefore, it is necessary to combine the design of low-curvature channels with interface chemical regulation[111].

Binder design

Binders play a critical role in maintaining particle-particle and particle-current-collector contact and thus preserving the mechanical and electronic integrity of graphite electrodes during repeated volume changes[112]. Conventional aqueous carboxymethyl cellulose/styrene-butadiene rubber (CMC/SBR) binder systems provide favorable dispersibility, flexibility, and adhesion, but their primarily mechanical function limits their ability to regulate interfacial chemistry. Functional binder design has therefore emerged as a strategy for simultaneously strengthening electrode cohesion and modifying the local electrode/electrolyte interface. Wang *et al*.[113] introduced Nafion as a functional additive into a commercial CMC/SBR binder system to regulate the interfacial structure of graphite anodes. Nafion contains sulfonic acid groups and fluorinated chain segments that can interact with Li^+ and participate in the formation of a more uniform and stable interfacial layer on the graphite surface. This structure helps suppress direct side reactions between solvated Li^+ and graphite and promotes the formation of a thin and uniform SEI with favorable Li^+ transport properties.

Consistent with this mechanism, transmission electron microscopy characterization after cycling revealed a relatively uniform and stable SEI for the CMC/SBR/Nafion electrode, whereas the conventional CMC/SBR system produced a thicker, cracked, and heterogeneous interphase. The incorporation of Nafion enabled the SEI to maintain greater structural stability during prolonged cycling. Binder engineering can also strengthen interparticle adhesion. Lim *et al*.[114] introduced polydopamine (PD) and polyacrylic acid (PAA) coatings onto graphite particles to enable *in situ* chemical crosslinking during dry electrode fabrication, thereby enhancing interparticle adhesion and mechanical stability. As illustrated in Figure 8C[114], unmodified dry-processed graphite electrodes (DP-bGr) are susceptible to contact loss, cracking, and delamination during cycling, whereas PD coating partially improves interparticle bonding. Further incorporation of PAA enables chemical crosslinking with PD, forming an interconnected three-dimensional network that reinforces electrode structural integrity. As shown in Figure 8D[114], graphite/NCM622 full cells using crosslinked graphite electrodes (DP-xPDAA@Gr) retained 87.1% of their initial capacity after 500 cycles at 1 C, outperforming PD-coated electrodes (84.0%) and unmodified dry-processed electrodes (77.9%). These results demonstrate that strengthening interparticle mechanical bonding can mitigate structural degradation and electronic contact loss during cycling, thereby improving the long-term stability of graphite anodes. Taken together, these studies show that the role of the binder extends well beyond simply holding the electrode together. Functional groups and crosslinkable structures introduced into the binder can interact with electrode components and electrolyte, while also improving particle-to-particle contact and accommodating the deformation of graphite during cycling. These functions become increasingly important as cycling proceeds, particularly under high-rate conditions where mechanical and interfacial degradation are more pronounced.

Three-dimensional conductive networks and gradient electrode architectures

For thick and high-loading graphite electrodes, simply increasing the amount of conductive additive or reducing electrode thickness is insufficient to overcome the coupled limitations of ionic and electronic transport. Three-dimensional conductive networks and spatially heterogeneous electrode architectures provide alternative approaches by independently tailoring transport pathways and local material composition across the electrode thickness. In principle, these architectures can simultaneously improve electronic conductivity, electrolyte accessibility, mechanical support, and current distribution.

Gradient electrodes are designed according to the distinct functional requirements of different regions within the electrode. Gradients in active material content, conductive additive fraction, or porosity can effectively alleviate volume expansion and stress concentration during cycling and thereby improve mechanical integrity. A bottom layer with a higher conductive additive content and a lower active material content is positioned near the current collector to enhance electron transport and interfacial adhesion to the current collector. A top layer with a higher active material content and greater porosity is positioned near the electrolyte to improve electrolyte wettability and ion transport while providing sufficient space to accommodate volume expansion[115]. Wang *et al.*[116] developed a three-dimensional carbon nanotube (CNT)-coated copper mesh composite current collector to improve interfacial adhesion and structural stability in graphite anodes. As illustrated in Figure 8E, graphite electrodes supported on conventional copper foil are susceptible to cracking and delamination during repeated cycling, while bare copper mesh provides insufficient mechanical support within its pores, resulting in active material cracking and detachment. In contrast, the CNT conductive network provides mechanical support for graphite within the copper mesh, enhances adhesion between the active material and current collector, and mitigates structural damage caused by repeated volume changes. As shown in Figure 8F, the graphite electrode using the composite current collector retained a specific capacity of 297.9 mAh g^{-1} after 200 cycles at 0.5 C, corresponding to 94.3% capacity retention, outperforming the conventional copper foil electrode (238.3 mAh g^{-1} and 81.2% retention). These results demonstrate that three-dimensional conductive current collectors can mitigate active material detachment and electronic contact loss, thereby improving the long-term cycling stability of graphite anodes.

In addition to constructing macroscopic gradients in porosity and active material content, establishing a three-dimensional network at the particle scale that provides both electrical conduction and mechanical support can also improve the cycling stability of composite anodes[117]. Li *et al.*[118] introduced CNTs into an artificial graphite matrix to construct a composite anode with a hierarchical conductive skeleton and multidirectional graphite microcrystalline structure. The CNTs formed continuous electronic transport networks between adjacent graphite domains, while the multidirectional graphite microcrystallites shortened the Li^+ diffusion pathways, thereby synergistically improving electronic and ionic transport within the electrode. The optimized graphite/CNT anode delivered a reversible capacity of 256 mAh g^{-1} at 5 C, substantially higher than the 126 mAh g^{-1} obtained for PG, and retained a capacity of 268 mAh g^{-1} after 800 cycles at 2 C. These results demonstrate that constructing a continuous three-dimensional conductive framework within graphite electrodes can improve electronic contact and Li^+ transport, thereby enhancing rate capability and cycling stability. Three-dimensional conductive additives provide another method to separate electron and ion transport within the electrode. He *et al.*[119] reported a reduced graphene oxide/Super P binary conductive additive. The reduced graphene oxide provides efficient two-dimensional electron conduction, and the Super P particles help to create additional pathways for ion transport. With this conductive architecture, $LiFePO_4$ and $LiCoO_2$ cells delivered specific capacities of 131.4 and 150.1 mAh g^{-1} at 5 C.

ADVANCED CHARACTERIZATION AND FUTURE PERSPECTIVES ON GRAPHITE ANODE FAILURE

Advanced characterization techniques have provided new ways to examine graphite degradation under electrochemical operation without relying solely on post-mortem analysis. Operando XRD and *in situ*/operando AFM are therefore useful from different perspectives, with the former mainly capturing changes in the bulk graphite structure and the latter providing information on the local graphite/electrolyte interface.

Operando XRD enables continuous tracking of the staging transitions of graphite during lithiation and delithiation under working conditions. Wang *et al*.[120] employed transmission operando XRD to investigate NCM811/graphite pouch cells and observed distinct differences in the phase evolution, structural changes, and relaxation behavior of graphite between 0.1 and 2.5 C, demonstrating that high-rate operation substantially alters the dynamic phase-transition behavior of graphite. Takagi *et al*.[121] further investigated the structural evolution of graphite during 5 C discharge using operando synchrotron radiation XRD. Several intermediate stages were kinetically bypassed during the transition from LiC_6 toward higher-stage structures, while the coexistence of multiple stage structures revealed pronounced reaction heterogeneity under high-rate conditions. After discharge, relaxation of the interlayer stage structure was also slower than that of the in-plane structure. These observations demonstrate that operando XRD can not only identify changes in graphite phase composition but also establish direct relationships among current density, reaction heterogeneity, and non-equilibrium structural evolution.

In situ/*operando* AFM can further resolve local dynamic changes at the graphite/electrolyte interface. Uebou *et al*.[122] employed *in situ* electrochemical AFM to investigate the evolution of the surface film on graphite under different temperature conditions. In $LiPF_6$-based electrolytes, localized blister-like structures formed at graphite step edges and subsequently enlarged, collapsed, and partially disrupted as the temperature increased, whereas the addition of vinylene carbonate or the use of LiFSI markedly improved the thermal stability of the interfacial film. These observations demonstrate that AFM can directly capture transient interfacial changes that are difficult to preserve through post-mortem characterization and correlate SEI evolution with temperature and electrolyte chemistry[122].

Future advanced characterization should move beyond visualization of individual failure phenomena toward quantitative analysis of coupled degradation mechanisms. Multimodal operando approaches capable of simultaneously tracking graphite phase transitions, SEI evolution, lithium plating, and local mechanical changes are needed to distinguish the relative contributions of different degradation pathways under different SOC, temperatures, and charging rates, and to establish causal relationships among interfacial chemistry, transport limitations, and mechanical evolution. Higher temporal and spatial resolution will also be required to directly correlate local structural and interfacial changes with electrochemical signals such as voltage, current, and impedance. More importantly, many current *in situ* studies still rely on thin electrodes, relatively low mass loadings, or specially designed cells. Future studies should therefore extend these diagnostic approaches to high-areal-capacity thick electrodes, lean-electrolyte conditions, and commercial-scale cells. Establishing quantitative correlations between laboratory-scale operando signals and the distributions of temperature, stress, and current density in practical cells will help advance the understanding of graphite-anode failure from qualitative description toward predictive diagnosis and provide more direct guidance for interfacial regulation and electrode design under fast-charging conditions.

CONCLUSIONS

In summary, the degradation of graphite anodes in LIBs originates from the dynamic coupling among SEI instability, lithium plating, and mechanical deterioration. During cycling, the volume changes of graphite generate mechanical stress, which continuously damages the anode/electrolyte interface and drives repetitive SEI fracture and reconstruction. The resulting accumulation of interfacial resistance and the loss of lithium further deteriorate Li^+ transport kinetics, intensify polarization, and increase the risk of lithium plating under fast charging and low-temperature operation. Meanwhile, deposited metallic lithium accelerates SEI degradation and induces additional mechanical damage, while particle cracking exposes new graphite surfaces and leads to electrolyte decomposition. Through these effects, degradation progressively propagates across multiple length scales, from atomic-scale interfacial reactions to particle fracture and electrode-level structural deterioration, ultimately resulting in capacity fading, impedance growth, and safety risks.

Recent research has developed multiple effective regulation strategies for graphite anode optimization. Electrolyte and interfacial engineering strategies regulate Li^+ solvation environments, SEI composition, and interfacial charge-transfer processes to suppress parasitic reactions and lithium plating. Graphite material modification, including carbon coating, interlayer spacing modulation, and elemental doping, focuses on optimizing lithium transport kinetics, surface chemistry, and structural robustness. Meanwhile, electrode architecture engineering, including pore-structure optimization, functional binder design, and three-dimensional conductive networks, aims to maintain homogeneous ion/electron transport and mechanical integrity during long-term cycling. These developments demonstrate that improving graphite anode performance requires not only optimization of individual components but also coordinated regulation across material, interface, and electrode scales.

Although existing optimization approaches have achieved promising results, many fundamental and practical obstacles still limit the application of graphite anodes. The dynamic evolution and mutual influences of SEI degradation, lithium plating and particle mechanical failure during cycling are still poorly understood. Several critical unresolved questions remain to be systematically addressed. Specifically, it remains challenging to quantitatively distinguish and decouple SEI growth from lithium plating during long-term cell aging, which hinders the accurate attribution of capacity decay. In addition, how local mechanical constraints alter interfacial ion transport behavior and further induce heterogeneous lithium plating remains unclear and lacks quantitative interpretation. Moreover, it is urgent to establish effective strategies to transfer laboratory-scale diagnostic signals and mechanistic understanding to practical commercial cells under realistic operating conditions. It is also difficult to determine the dominant degradation pathway under varied temperatures, charging rates, and electrode loading conditions, which makes it impossible to explain complex failure behaviors with a single mechanism. Clarifying these coupled interfacial and structural changes requires high-resolution operando characterization tools and multiscale models that connect interfacial reactions to particle and electrode-level structural evolution. Future research should focus more on building quantitative correlations between microscopic degradation behaviors and macroscopic cell performance and validating modification strategies under realistic electrode manufacturing and operating conditions. Next-generation graphite anode development no longer relies on the simple optimization of a single material or interfacial property. It requires comprehensive regulation of the coupled electrochemical, mechanical, and mass transport behaviors throughout long-term cycling.

DECLARATIONS

Authors' contributions

Substantial contributions to the conception and design of the study: Song, X.; Chen, Q.
Project administration: Wang, J.
Assistance in the design of the study, manuscript editing, and administrative support: Zhao, J.; Zhao, Z.; Liu, X.
Manuscript drafting and editing and technical support: Chen, J.; Ji, J.

Availability of data and materials

Not applicable.

AI and AI-assisted tools statement

Not applicable.

Financial support and sponsorship

This work was financially supported by the National Natural Science Foundation of China (52301282), Key Technologies R&D Program of Shanxi Province (202502060302013, 202501060302002), Natural Science Foundation of Shanxi Province (No. 202303021212047, 202303021212044), and Shanxi Provincial Science and Technology Cooperation and Exchange Special Project (202504041101043).

Conflicts of interest

Zhao, Z. and Liu, X. are affiliated with CNOOC (Shanxi) Precious Metals Co., Ltd., while the other authors have declared that they have no conflicts of interest.

Ethical approval and consent to participate

Not applicable.

Consent for publication

Not applicable.

Copyright

© The Author(s) 2026.

REFERENCES

1. Wang, Y.; Leau, C.; Coudray, S.; et al. Formation dynamics of an ethylene carbonate-derived solid-electrolyte-interphase in commercial Li-ion batteries. *Energy. Environ. Sci.* **2026**, *19*, 619-34. DOI
2. Bisht, A.; Dixit, M. B.; Burson, A.; Preefer, M. B.; Kweon, C. B. M.; Belharouak, I. Low-rate cycling regeneration sustains NMC811-graphite battery performance through extreme ultrafast charging. *ACS. Energy. Lett.* **2026**, *11*, 4325-33. DOI
3. Li, M.; Lu, D.; Wang, J.; et al. Solvation sheath reorganization enables fast ion transfer kinetics in lithium-ion battery. *Nat. Commun.* **2026**, *17*, 3953. DOI PubMed PMC
4. Han, J.; Phillips, G. S.; Merryweather, A. J.; et al. Avalanche-like intercalation and intraparticle correlations in graphite. *Nature* **2026**, *656*, 364-9. DOI PubMed PMC
5. Bhattacharyya, S.; Roy, S.; Lin, X.; Campagnol, N.; Vlad, A.; Ajayan, P. M. Graphite: the new critical mineral. *Nat. Rev. Mater.* **2026**, *11*, 65-78. DOI
6. Jia, A.; Gao, W.; Wang, J.; et al. Suppressed lithium plating in graphite anodes enabled by tailoring the interfacial lithium concentration. *Joule* **2026**, *10*, 102278. DOI
7. Wen, F.; Peng, Y.; Ding, M.; et al. Calendar aging of $LiFePO_4$/graphite batteries: quantitative analysis of synergistic effects of SEI evolution and electrolyte decomposition. *ACS. Energy. Lett.* **2026**, *11*, 489-97. DOI
8. Mo, C.; Wu, H.; Chen, S.; et al. Dehydrating a borate additive unlocks fast-charging graphite. *Adv. Energy. Mater.* **2026**, *16*, e71230. DOI
9. Lin, J.; Hu, W.; Yang, J.; et al. Quantifying aging kinetics in $LiFePO_4$/graphite pouch cells: cycle aging vs calendar aging via a novel impedance descriptor. *Energy. Storage. Mater.* **2026**, *86*, 104926. DOI
10. Che, L.; Zhang, K.; Hu, Z.; et al. Heterohalogenated hybrid SEI reconstructs graphite anode interfacial kinetics at low temperatures. *ACS. Energy. Lett.* **2026**, *11*, 2152-61. DOI
11. Song, J.; Ji, W.; Xu, C.; et al. Interfacial chemistry regulation via $AlPO_4$ modification enables fast charging and wide-temperature operation of graphite anodes for lithium-ion batteries. *Adv. Energy. Mater.* **2026**, e71158. DOI
12. Liu, X.; Zhang, J.; Li, J.; et al. Steric coordinated electrolytes for fast-charging and low-temperature energy-dense lithium-ion batteries. *Angew. Chem. Int. Ed.* **2025**, *64*, e202502978. DOI PubMed
13. Yoo, H.; Lim, J.; Hwang, J. H.; Oh, S.; Lee, Y. M.; Kim, H. Porosity-gradient dry-processed graphite electrode with deformable primer layer for boosting fast-charging capability of lithium-ion batteries. *Energy. Storage. Mater.* **2026**, *90*, 105331. DOI
14. Dong, Y.; Wu, F.; Chen, T.; et al. Hierarchically conformal Li^+/electron conductive and mechanically robust interface enabling natural graphite anodes for fast-charging and long-cycling operation. *Adv. Energy. Mater.* **2025**, *15*, 2500978. DOI
15. Lin, H.; Liu, F.; Yang, E.; et al. Tailoring graphite interfacial chemistry with medium concentration weakly solvating electrolyte toward fast-charging and low-temperature lithium-ion batteries. *Nano. Energy.* **2025**, *142*, 111266. DOI
16. Zhang, Z.; Wang, M.; Wang, X.; et al. Cathode-dependent electrochemical-mechanical coupling governing edge lithium plating and interfacial void heterogeneity of lithium-ion batteries. *Adv. Energy. Mater.* **2026**, *16*, e71300. DOI
17. Sun, N.; Rong, Q.; Wu, J.; et al. Fully printable integrated multifunctional sensor arrays for intelligent lithium-ion batteries. *Nat. Commun.* **2025**, *16*, 7361. DOI PubMed PMC
18. Wang, W.; Liu, S.; Yang, Y.; et al. Quantitatively mapping inhomogeneous state of charge in a commercial lithium-ion pouch cell via energy-resolved neutron imaging. *ACS. Energy. Lett.* **2025**, *10*, 3359-66. DOI
19. Wang, Y.; Feng, H.; Zhang, C.; Liu, Q.; Tan, J.; Ye, C. Interlayer nanoarchitecture modification of layered materials in rechargeable metal-ion batteries. *Electrochem. Energy. Rev.* **2025**, *8*, 19. DOI

20. Ohzuku, T.; Iwakoshi, Y.; Sawai, K. Formation of lithium-graphite intercalation compounds in nonaqueous electrolytes and their application as a negative electrode for a lithium ion (shuttlecock) cell. *J. Electrochem. Soc.* **1993**, *140*, 2490. DOI
21. Xu, Q.; Guo, L.; Yu, H.; et al. Electronegative interface modification enables accelerated interfacial kinetics for lithium-ion battery anodes. *Carbon* **2025**, *244*, 120638. DOI
22. Strobl, M.; Baur, M. E.; Samothrakitis, S.; et al. Concurrent operando neutron imaging and diffraction analysis revealing spatial lithiation phase evolution in an ultra-thick graphite electrode. *Adv. Energy. Mater.* **2025**, *15*, 2405238. DOI
23. Xu, H.; Li, H.; Wang, X. The anode materials for lithium-ion and sodium-ion batteries based on conversion reactions: a review. *ChemElectroChem* **2023**, *10*, e202201151. DOI
24. Renais, C.; Villevieille, C.; Peljo, P.; El Bachraoui, F.; Girault, H. Redox aspects of lithium-ion batteries. is graphite an anode? *EES. Batteries.* **2026**, *2*, 103-11. DOI
25. Waldmann, T.; Hogg, B. I.; Wohlfahrt-Mehrens, M. Li plating as unwanted side reaction in commercial Li-ion cells - a review. *J. Power. Sources.* **2018**, *384*, 107-24. DOI
26. He, X.; Zheng, S.; Sun, K.; et al. Operando electrode-scale stress characterization revealing the Li^+ insertion mechanism of graphite anode. *Energy. Storage. Mater.* **2025**, *82*, 104629. DOI
27. Kang, Y.; Jang, S.; Kim, H.; Park, J.; Lee, K. T. Digital twin-driven insights into electrochemical, mechanical and microstructural interactions of lithium-ion battery anode. *Chem. Eng. J.* **2025**, *518*, 164524. DOI
28. Wang, X.; Hu, B.; Cao, X.; et al. Edge-engineered graphite modulates SEI formation and enables fast-charging lithium-ion batteries. *Chem. Eng. J.* **2026**, *529*, 173048. DOI
29. Peled, E.; Menkin, S. Review—SEI: past, present and future. *J. Electrochem. Soc.* **2017**, *164*, A1703. DOI
30. Gauthier, M.; Carney, T. J.; Grimaud, A.; et al. Electrode-electrolyte interface in Li-ion batteries: current understanding and new insights. *J. Phys. Chem. Lett.* **2015**, *6*, 4653-72. DOI PubMed
31. Tan, J.; Ma, L.; Li, Z.; Wang, Y.; Ye, M.; Shen, J. Structural insights into solid electrolyte interphase (SEI) on lithium metal anode: from design strategies to the stability evaluation. *Mater. Today.* **2023**, *69*, 287-332. DOI
32. Liu, T.; Lin, L.; Bi, X.; et al. In situ quantification of interphasial chemistry in Li-ion battery. *Nat. Nanotechnol.* **2019**, *14*, 50-6. DOI PubMed
33. Ding, J. F.; Xu, R.; Yan, C.; Li, B. Q.; Yuan, H.; Huang, J. Q. A review on the failure and regulation of solid electrolyte interphase in lithium batteries. *J. Energy. Chem.* **2021**, *59*, 306-19. DOI
34. Single, F.; Latz, A.; Horstmann, B. Identifying the mechanism of continued growth of the solid-electrolyte interphase. *ChemSusChem* **2018**, *11*, 1950-5. DOI PubMed
35. An, S. J.; Li, J.; Daniel, C.; Mohanty, D.; Nagpure, S.; Wood, D. L. The state of understanding of the lithium-ion-battery graphite solid electrolyte interphase (SEI) and its relationship to formation cycling. *Carbon* **2016**, *105*, 52-76. DOI
36. Leung, K.; Budzien, J. L. Ab initio molecular dynamics simulations of the initial stages of solid-electrolyte interphase formation on lithium ion battery graphitic anodes. *Phys. Chem. Chem. Phys.* **2010**, *12*, 6583-6. DOI PubMed
37. Wang, A.; Kadam, S.; Li, H.; Shi, S.; Qi, Y. Review on modeling of the anode solid electrolyte interphase (SEI) for lithium-ion batteries. *npj. Comput. Mater.* **2018**, *4*, 15. DOI
38. Lin, Y. X.; Liu, Z.; Leung, K.; Chen, L. Q.; Lu, P.; Qi, Y. Connecting the irreversible capacity loss in Li-ion batteries with the electronic insulating properties of solid electrolyte interphase (SEI) components. *J. Power. Sources.* **2016**, *309*, 221-30. DOI
39. Smeu, M.; Leung, K. Electron leakage through heterogeneous LiF on lithium-metal battery anodes. *Phys. Chem. Chem. Phys.* **2021**, *23*, 3214-8. DOI PubMed
40. Li, J.; Adewuyi, K.; Lotfi, N.; Landers, R. G.; Park, J. A single particle model with chemical/mechanical degradation physics for lithium ion battery state of health (SOH) estimation. *Appl. Energy.* **2018**, *212*, 1178-90. DOI
41. Edge, J. S.; O'Kane, S.; Prosser, R.; et al. Lithium ion battery degradation: what you need to know. *Phys. Chem. Chem. Phys.* **2021**, *23*, 8200-21. DOI PubMed
42. Lin, N.; Jia, Z.; Wang, Z.; et al. Understanding the crack formation of graphite particles in cycled commercial lithium-ion batteries by focused ion beam - scanning electron microscopy. *J. Power. Sources.* **2017**, *365*, 235-9. DOI
43. Aurbach, D.; Gamolsky, K.; Markovsky, B.; Gofer, Y.; Schmidt, M.; Heider, U. On the use of vinylene carbonate (VC) as an additive to electrolyte solutions for Li-ion batteries. *Electrochim. Acta.* **2002**, *47*, 1423-39. DOI
44. Zhang, K.; Hu, Y.; Tang, S.; et al. Decoupling electrolyte degradation pathways with diverse Li plating processes on graphite electrodes. *Adv. Energy. Mater.* **2026**, *16*, e05230. DOI
45. Gachot, G.; Grugeon, S.; Eshetu, G. G.; et al. Thermal behaviour of the lithiated-graphite/electrolyte interface through GC/MS analysis. *Electrochim. Acta.* **2012**, *83*, 402-9. DOI
46. Park, H.; Yoon, T.; Kim, Y.; et al. Thermal behavior of solid electrolyte interphase films deposited on graphite electrodes with different states-of-charge. *J. Electrochem. Soc.* **2015**, *162*, A892. DOI

47. Zhu, H.; Russell, J. A.; Fang, Z.; et al. A comparison of solid electrolyte interphase formation and evolution on highly oriented pyrolytic and disordered graphite negative electrodes in lithium-ion batteries. *Small* **2021**, *17*, 2105292. DOI PubMed
48. Solchenbach, S.; Hong, G.; Freiberg, A. T. S.; Jung, R.; Gasteiger, H. A. Electrolyte and SEI decomposition reactions of transition metal ions investigated by on-line electrochemical mass spectrometry. *J. Electrochem. Soc.* **2018**, *165*, A3304. DOI
49. Ferrero, G. A.; Åvall, G.; Janßen, K.; et al. Solvent Co-intercalation reactions for batteries and beyond. *Chem. Rev.* **2025**, *125*, 3401-39. DOI PubMed PMC
50. Ming, J.; Cao, Z.; Wahyudi, W.; et al. New insights on graphite anode stability in rechargeable batteries: Li ion coordination structures prevail over solid electrolyte interphases. *ACS. Energy. Lett.* **2018**, *3*, 335-40. DOI
51. Wang, R.; Wang, H.; Zhao, H.; et al. Highly fluorinated co-solvent enabling ether electrolyte for high-voltage lithium ion batteries with graphite anode. *Energy. Mater.* **2023**, *3*, 300040. DOI
52. Luchkin, S. Y.; Pazhetnov, E. M. Explaining the EC-PC disparity in Li-ion batteries: how interface stiffness governs SEI formation on graphite. *J. Mater. Chem. A.* **2024**, *12*, 29795-801. DOI
53. Chen, C.; Che, L.; Shen, C.; et al. Topological structure design of ether solvents for lithium storage chemistry in graphite anode. *Angew. Chem. Int. Ed.* **2026**, *65*, e14696. DOI PubMed
54. Yan, X.; Chen, K.; Chen, Z.; Ai, X.; Cao, Y. Uncoupling solvent cointercalation on graphite anode in lithium-ion batteries. *Adv. Energy. Mater.* **2026**, *16*, e05287. DOI
55. Li, Z.; Yang, Z. J.; Chhowalla, M. Stabilising graphite anode with quasi-solid-state electrolyte for long-life lithium-sulfur batteries. *MRS. Energy. Sustain.* **2025**, *12*, 262-9. DOI PubMed PMC
56. Chen, Y.; Xuan, W.; Zhang, W.; et al. Hidden subsurface molecular bubbles in graphite anodes for LIBs. *Energy. Environ. Sci.* **2025**, *18*, 8430-45. DOI
57. Gao, T.; Han, Y.; Fraggedakis, D.; et al. Interplay of lithium intercalation and plating on a single graphite particle. *Joule* **2021**, *5*, 393-414. DOI
58. Zhang, S. S. Challenges and strategies for fast charge of Li-ion batteries. *ChemElectroChem* **2020**, *7*, 3569-77. DOI
59. Hu, D.; Chen, L.; Tian, J.; et al. Research progress of lithium plating on graphite anode in lithium-ion batteries. *Chin. J. Chem.* **2021**, *39*, 165-73. DOI
60. Chen, H.; Lu, G.; Cao, Z.; et al. MXene-configured graphite towards long-life lithium-ion batteries under extreme conditions. *Nat. Commun.* **2025**, *16*, 8493. DOI PubMed PMC
61. Hu, D.; Chen, G.; Tian, J.; et al. Unrevealing the effects of low temperature on cycling life of 21700-type cylindrical Li-ion batteries. *J. Energy. Chem.* **2021**, *60*, 104-10. DOI
62. Kirchner-Burles, C.; Fordham, A.; Reid, H. T.; et al. Safety and performance implications of lithium plating induced by sub-zero temperature cycling of lithium-ion batteries. *J. Power. Sources.* **2025**, *660*, 238565. DOI
63. Cheng, M.; Chen, A.; Zhang, Z.; Sheng, C.; Zhou, H.; He, P. Regulating lithium intercalation/plating competition to enhance low-temperature performance of Li-ion batteries. *J. Am. Chem. Soc.* **2025**, *147*, 40776-87. DOI PubMed
64. Chen, B.; Hope-Glenn, N.; Wright, A.; Messinger, R. J.; Couzis, A. Mechanistic understanding of lithium-ion adsorption, intercalation, and plating during charging of graphite electrodes. *ACS. Electrochem.* **2025**, *1*, 574-87. DOI PubMed PMC
65. Mao, S.; Wang, Y.; Lu, Y.; et al. In situ evaluation and manipulation of lithium plating morphology enabling safe and long-life lithium-ion batteries. *InfoMat* **2025**, *7*, e12612. DOI
66. Shkrob, I. A.; Rodrigues, M. T. F.; Abraham, D. P. Fast charging of Li-ion cells: part III. relaxation dynamics and trap-controlled lithium ion transport. *J. Electrochem. Soc.* **2019**, *166*, A4168. DOI
67. Colclasure, A. M.; Dunlop, A. R.; Trask, S. E.; Polzin, B. J.; Jansen, A. N.; Smith, K. Requirements for enabling extreme fast charging of high energy density Li-ion cells while avoiding lithium plating. *J. Electrochem. Soc.* **2019**, *166*, A1412. DOI
68. von Lüders, C.; Zinth, V.; Erhard, S. V.; et al. Lithium plating in lithium-ion batteries investigated by voltage relaxation and in situ neutron diffraction. *J. Power. Sources.* **2017**, *342*, 17-23. DOI
69. Huang, W.; Ye, Y.; Chen, H.; et al. Onboard early detection and mitigation of lithium plating in fast-charging batteries. *Nat. Commun.* **2022**, *13*, 7091. DOI PubMed PMC
70. Peng, Y.; Ding, M.; Zhang, K.; et al. Quantitative analysis of the coupled mechanisms of lithium plating, SEI growth, and electrolyte decomposition in fast charging battery. *ACS. Energy. Lett.* **2024**, *9*, 6022-8. DOI
71. Abe, Y.; Kumagai, S. Effect of negative/positive capacity ratio on the rate and cycling performances of $LiFePO_4$/graphite lithium-ion batteries. *J. Energy. Storage.* **2018**, *19*, 96-102. DOI
72. Kim, S.; Lee, D.; Han, Y.; Kim, H. W.; Yoo, D. J. Abnormal lithium plating in the electrode edges at low N/P ratios in lithium-ion batteries. *J. Power. Sources.* **2024**, *601*, 234301. DOI
73. Roth, T.; Frank, A.; Oehler, F.; Graule, A.; Kücher, S.; Jossen, A. Lithium plating at the cell edge induced by anode overhang during cycling in lithium-ion batteries: part I. modeling and mechanism. *J. Electrochem. Soc.* **2024**, *171*, 050547. DOI

74. Chen, F.; Chen, T.; Lu, K.; et al. Three-dimensional electrochemical-thermodynamic modeling reveals manufacturing defect mechanisms governing lithium plating in lithium-ion batteries. *Chem. Eng. J.* **2025**, *521*, 166887. DOI
75. Yang, X. G.; Bauer, C.; Wang, C. Y. Sinusoidal current and stress evolutions in lithium-ion batteries. *J. Power. Sources.* **2016**, *327*, 414-22. DOI
76. Li, D.; Zhu, G.; Liu, H.; Wang, Y. Diffusion-induced stress in commercial graphite electrodes during multiple cycles measured by an in situ method. *Micromachines* **2022**, *13*, 142. DOI PubMed PMC
77. Liu, J.; Gu, H.; Jiang, H.; et al. In-situ study of lithium insertion on the electrochemical-mechanical coupling behavior of graphite composite electrodes. *Energy. Mater.* **2025**, *5*, 500054. DOI
78. Schweidler, S.; de Biasi, L.; Schiele, A.; Hartmann, P.; Brezesinski, T.; Janek, J. Volume changes of graphite anodes revisited: a combined operando X-ray diffraction and in situ pressure analysis study. *J. Phys. Chem. C.* **2018**, *122*, 8829-35. DOI
79. Takahashi, K.; Srinivasan, V. Examination of graphite particle cracking as a failure mode in lithium-ion batteries: a model-experimental study. *J. Electrochem. Soc.* **2015**, *162*, A635. DOI
80. Marin-Montin, J.; Zurita-Gotor, M.; Montero-Chacón, F. A numerical study of mechanical degradation of carbon-coated graphite active particles in Li-ion battery anodes. *J. Electrochem. Soc.* **2022**, *169*, 070528. DOI
81. Sarkar, A.; Shrotriya, P.; Nlebedim, I. C. Parametric analysis of anodic degradation mechanisms for fast charging lithium batteries with graphite anode. *Comput. Mater. Sci.* **2022**, *202*, 110979. DOI
82. Xu, Z.; Shi, X.; Zhuang, X.; et al. Chemical strain of graphite-based anode during lithiation and delithiation at various temperatures. *Research* **2021**, *2021*, 9842391. DOI PubMed PMC
83. Sun, Z.; Dai, R.; Zhang, S.; Xia, Y.; Zhou, Q. Microscale analysis on cycling aging effect in mechanical behavior of graphite anode coating: morphological statistics and nanoindentation. *J. Energy. Storage.* **2025**, *116*, 116088. DOI
84. Pietsch, P.; Westhoff, D.; Feinauer, J.; et al. Quantifying microstructural dynamics and electrochemical activity of graphite and silicon-graphite lithium ion battery anodes. *Nat. Commun.* **2016**, *7*, 12909. DOI PubMed PMC
85. Suthar, B.; Northrop, P. W. C.; Rife, D.; Subramanian, V. R. Effect of porosity, thickness and tortuosity on capacity fade of anode. *J. Electrochem. Soc.* **2015**, *162*, A1708. DOI
86. Ren, Z.; Shen, D.; Ji, Y.; et al. Exploring lithium-ion diffusion and electronic properties in defective graphite via molecular dynamics and density functional theory. *J. Chem. Phys.* **2025**, *163*, 064704. DOI PubMed
87. Marin-Montin, J.; Zurita-Gotor, M.; Montero-Chacón, F. Numerical analysis of degradation and capacity loss in graphite active particles of Li-ion battery anodes. *Materials* **2022**, *15*, 3979. DOI PubMed PMC
88. Nasiri, S.; Zaiser, M. Rupture of graphene sheets with randomly distributed defects. *AIMS. Mater. Sci.* **2016**, *3*, 1340-9. DOI
89. Pinson, M. B.; Bazant, M. Z. Theory of SEI formation in rechargeable batteries: capacity fade, accelerated aging and lifetime prediction. *J. Electrochem. Soc.* **2013**, *160*, A243. DOI
90. Chen, S.; Liu, C.; Feng, R.; et al. Natural graphite anode for advanced lithium-ion batteries: challenges, progress, and perspectives. *Chem. Eng. J.* **2025**, *503*, 158116. DOI
91. Xiao, P.; Wang, Z.; Long, K.; et al. Stable cycling and low-temperature operation utilizing amorphous carbon-coated graphite anodes for lithium-ion batteries. *RSC. Adv.* **2024**, *14*, 13277-85. DOI PubMed PMC
92. Ma, H.; Yin, B.; Ye, T.; et al. Constructing lithiophilic coating layer on the natural graphite for high-rate lithium-ion batteries. *Electrochim. Acta.* **2025**, *527*, 146275. DOI
93. Zhang, C.; Huang, X.; Xiao, T.; et al. The interlayer spacing regulation with good universality for artificial graphite. *Chem. Eng. Sci.* **2026**, *320*, 122423. DOI
94. Zha, H.; Zhang, X.; Li, X.; et al. In situ alkali metal exfoliation-coupled dilute CO_2 electrolysis to synthesize interlayer-expanded graphite for high-rate lithium storage. *Adv. Sci.* **2026**, *13*, e76734. DOI PubMed PMC
95. Rathi, K.; Pakharenko, V.; Titton Dias, O. A.; van der Kuur, C.; Yan, N.; Sain, M. One-step dual process strategy for holey graphite towards scalable and stable lithium-ion battery anodes. *J. Mater. Chem. A.* **2025**, *13*, 36564-36575. DOI
96. Liu, Y.; Shi, H.; Yang, M.; et al. Kilogram-scale production of ultrafast-charging micro-expanded graphite anode toward high-power and long-life Ah-level pouch batteries. *Adv. Mater.* **2025**, *37*, e06584. DOI PubMed
97. Ghorbani Shadpey, F.; Soleimani, M.; Pourfath, M. First-principles insights into Li storage and ion diffusion in B-, P-, and S-doped C_2N anodes. *ACS. Omega.* **2026**, *11*, 22007-16. DOI PubMed PMC
98. Huo, L.; Su, F.; Yi, Z.; et al. The inhibition mechanism of lithium dendrite on nitrogen-doped defective graphite: the first principles studies. *J. Electrochem. Soc.* **2019**, *166*, A1603. DOI
99. Chen, J. J.; Xu, Y.; Zhao, Z. X.; et al. An electron-rich sulfur host for advanced Zn-S batteries. *New. Carbon. Mater.* **2025**, *40*, 1074-84. DOI
100. Wang, Q.; Wang, J.; Heringa, J. R.; Bai, X.; Wagemaker, M. High-entropy electrolytes for lithium-ion batteries. *ACS. Energy. Lett.* **2024**, *9*, 3796-806. DOI PubMed PMC

101. Luo, Z.; Wang, Y.; Huang, Y.; Luo, H.; Lin, Z. Designing high-chaos mixed-salt electrolytes for enhancing graphite-electrolyte interfacial stability in lithium-ion batteries. *J. Power. Sources.* **2024**, *607*, 234611. DOI
102. Raj, M. R.; Zarei-Jelyani, M.; Maghsoudi, R.; Ganjali, F.; Salehi, A. H. Elucidating the low-temperature performance variations of graphite anode using different types of Li-based electrolyte salts: comparative study of $LiPF_6$, $LiBF_4$ and LiDFOB electrolytes. *J. Power. Sources.* **2026**, *676*, 239895. DOI
103. Zheng, Y.; Li, J.; Zhang, T.; et al. A weak-solvation strategy for modulating Li ion solvation sheath to enable fast-charging Li-ion batteries. *J. Colloid. Interface. Sci.* **2026**, *713*, 140177. DOI PubMed
104. Tao, L.; Zhang, H.; Shah, S. R.; et al. Revealing the roles of the solid-electrolyte interphase in designing stable, fast-charging, low-temperature Li-ion batteries. *Proc. Natl. Acad. Sci. USA.* **2025**, *122*, e2420398122. DOI PubMed PMC
105. Luo, L.; Chen, K.; Chen, H.; et al. Enabling ultralow-temperature (-70 °C) lithium-ion batteries: advanced electrolytes utilizing weak-solvation and low-viscosity nitrile cosolvent. *Adv. Mater.* **2024**, *36*, 2308881. DOI PubMed
106. Chen, Y.; He, Q.; Zhao, Y.; et al. Breaking solvation dominance of ethylene carbonate via molecular charge engineering enables lower temperature battery. *Nat. Commun.* **2023**, *14*, 8326. DOI PubMed PMC
107. Liu, J.; Wang, X.; Sha, L.; et al. Rechargeable organic coating as an artificial solid electrolyte interphase enabling high-capacity and fast-charging graphite anodes. *Energy. Storage. Mater.* **2025**, *81*, 104518. DOI
108. Weng, S.; Yang, G.; Zhang, S.; et al. Kinetic limits of graphite anode for fast-charging lithium-ion batteries. *Nanomicro. Lett.* **2023**, *15*, 215. DOI PubMed PMC
109. Moon, H.; Chava, R. K.; Mandari, K. K.; et al. Nitrogen-stitched rGO/graphite bilayer anodes for accelerated Li-ion transport and interfacial charge regulation. *Carbon. Energy.* **2026**, e70268. DOI
110. Ahmadi, S.; Maddipatla, D.; Bazuin, B. J.; Atashbar, M. Z. A comprehensive experimental study on microstructure-graded graphite anodes for enhancing fast-charging capability of lithium-ion batteries. *Adv. Energy. Sustain. Res.* **2024**, *5*, 2300213. DOI
111. Jiang, Q.; Cao, R.; Luo, J.; Fang, Y.; Chen, Z.; Cao, Y. Design of gradient porosity architecture with through-hole carbon spheres to promoting fast charging and low-temperature workable lithium-ion batteries. *Adv. Energy. Mater.* **2025**, *15*, 2403164. DOI
112. Lin, C.; Ajdari, F. B.; Mao, C.; et al. Functional binders in lithium batteries: from molecular structure design to practical applications. *Mater. Sci. Eng. R. Rep.* **2026**, *168*, 101142. DOI
113. Wang, H.; Qin, N.; Li, Y.; et al. Nafion as a facile binder additive stabilizes solid electrolyte interphase on graphite anode. *Carbon* **2023**, *205*, 435-43. DOI
114. Lim, J.; Kang, K.; Choi, S.; et al. In-situ crosslinkable graphite for mechanically robust dry-processed lithium-ion battery electrodes. *Carbon. Neutraliz.* **2025**, *4*, e70050. DOI
115. He, R.; Zhong, W.; Wu, Y.; et al. Two-layer graphite anode for energy and power densified $LiFePO_4$ battery. *Adv. Mater.* **2025**, *37*, 2501185. DOI PubMed
116. Wang, F.; Jin, S.; Meng, J.; et al. Three-dimensional carbon nanotube-coated copper mesh as a current collector for graphite anodes in high-performance lithium-ion batteries. *Processes* **2025**, *13*, 964. DOI
117. Gao, Y.; Zhang, Q.; Ni, Y.; et al. Silicon embedded into graphite by van der Waals force for high-performance Li-ion batteries. *Energy. Storage. Mater.* **2026**, *90*, 105382. DOI
118. Li, X.; Yuan, W.; Tian, Y.; et al. Construction of hierarchical conductive skeleton-multidirectional graphite microcrystalline structure for fast-charging lithium-ion batteries. *Chem. Eng. J.* **2026**, *547*, 181288. DOI
119. He, L.; Peng, J.; Liu, P.; et al. Topology-optimized binary composite conductive additive enabling 3D percolation networks for high-rate capability lithium-ion battery. *J. Energy. Storage.* **2025**, *137*, 118699. DOI
120. Wang, J.; Gao, Y.; Liu, J.; Liao, H.; Wang, L.; He, X. Operando X-ray diffraction boosting understanding of graphite phase evolution in lithium-ion batteries. *Small. Methods.* **2024**, *8*, 2301084. DOI PubMed
121. Takagi, S.; Shimoda, K.; Kiuchi, H.; Hase, K.; Ogumi, Z.; Abe, T. Phase transition analysis of graphite electrode during high-rate discharging by operando synchrotron radiation X-ray diffraction. *Carbon* **2025**, *238*, 120204. DOI
122. Uebou, Y.; Sato, Y.; Sasaki, T. Direct observation of cycle and temperature effects on surface film morphology of graphite negative electrode by in-situ electrochemical AFM. *Electrochem* **2025**, *93*, 063004. DOI

Disclaimer/Publisher's Note: All statements, opinions, and data contained in this publication are solely those of the individual author(s) and contributor(s) and do not necessarily reflect those of OAE and/or the editor(s). OAE and/or the editor(s) disclaim any responsibility for harm to persons or property resulting from the use of any ideas, methods, instructions, or products mentioned in the content.



© The Author(s) 2026. Open Access This article is licensed under a Creative Commons Attribution 4.0 International License (https://creativecommons.org/licenses/by/4.0/), which permits unrestricted use, sharing, adaptation, distribution and reproduction in any medium or format, for any purpose, even commercially, as long as you give appropriate credit to the original author(s) and the source, provide a link to the Creative Commons license, and indicate if changes were made.